Characterizing the role of *ice1* in maintaining zebrafish neural stem cells

by

Cassandra Marie D'Amata

A thesis submitted in conformity with the requirements
for the degree of Master of Science

Department of Cell and Systems Biology
University of Toronto

Characterizing the role of *ice1* in maintaining zebrafish neural stem cells

Cassandra Marie D'Amata

Master of Science

Department of Cell and Systems Biology
University of Toronto

2017

Abstract

Maintenance of neural stem cell (NSC) niches is required for the continued growth of the zebrafish retina and forebrain after embryogenesis. The zebrafish mutant *kes*^{s564}, which maps to the *ice1* locus, exhibits reduced NSC niches. RNA polymerase II-dependent snRNA transcription requires the little elongation complex (LEC) for which ICE1 is an essential scaffolding component. Mutant NSCs which are normally active no longer express markers of cycling cells and become apoptotic. Furthermore, quiescent NSCs of the mutant retina are unable to dedifferentiate in response to UV lesion. Whole-transcriptome analysis of *ice1* mutant larvae show a decrease in CNS and cell cycle levels, and an increase in splicing genes indicative of a possible compensatory mechanism. snRNA transcript levels appear to be unaffected in a subset of NSCs but reduced in differentiated neurons. This work demonstrates that *ice1* is essential for NSC maintenance in an *in vivo* loss of function model.

Acknowledgements

I would first and foremost like to thank my supervisor, Dr. Vince Tropepe, for giving me the opportunity to work on a project which I have found both wonderfully challenging and incredibly fulfilling. I deeply appreciate all of your support and encouragement throughout my candidacy. Thank you to my supervisory committee, Dr. Belinda Chang and Dr. Bret Pearson, for your feedback and insight in helping me shape my project. A special thank you to Dr. Ashley Bruce, who has been nothing short of inspirational, and to Dr. John Calarco, who has always had an open door for me.

I would like to thank everyone from the Tropepe lab – Monica, Zach, Steve, and Amanda – without whom none of this work would be possible. You all have been an immense help not just in sharing your knowledge, but in making the lab a great place to be every day. A huge thank you also to the Bruce and Winklbauer labs for your friendship over the past two years. Grad school would not have been the same, or nearly as much fun, without you all.

Above all, I thank my family and friends who have been absolute pillars of support throughout my life, and exceptionally so over the past two years. All the words of love and encouragement from my caring family, from my amazing friends Baula and Rick, and from my incredible boyfriend David, kept me pushing through to the end.

I dedicate this thesis to my sister, Stephanie, who is the most intelligent, driven, and inspiring woman that I know, and of whom I am immensely proud.

Table of Contents

List of Figures

List of Tables

List of Acronyms

CMZ. ..... Ciliary marginal zone

ChIP. ..... Chromatin immunoprecipitation

DNA. ..... Deoxyribonucleic acid

dpf. ..... Days post fertilization

FACS..... Fluorescence-activated cell sorting

FBS. ..... Fetal bovine serum

hpl. ..... Hours post lesion

INL. ..... Inner nuclear layer

LEC. ..... Little elongation complex

ONL. ..... Outer nuclear layer

PBS. ..... Phosphate buffered saline

PCR. ..... Polymerase chain reaction

PVZ. ..... Periventricular zone

RNA. ..... Ribonucleic acid

RPE. ..... Retinal pigmented epithelium

RT-qPCR..... Real time quantitative PCR

SEC. ..... Super elongation complex

snRNA..... Small nuclear RNA

snRNP. ..... Small nuclear ribonucleoprotein

UV. ..... Ultraviolet

3' UTR. ..... 3-prime untranslated region

Chapter 1
Introduction

The mammalian nervous system has limited capacity for regeneration *in vivo* (Ming and Song 2005). Consequently, any damage to the retina or brain in the form of physical injury or neurodegenerative disease is usually permanent. In contrast, some vertebrates, such as zebrafish, are able to continually generate new neurons in the retina and brain into adulthood as well as regenerate these tissues in response to damage (Marcus et al. 1999; Fischer et al. 2013). In the retina, this is largely due to an actively dividing stem cell population located in the ciliary marginal zone (CMZ), and the ability of radial glia in the central retina to dedifferentiate into multipotent stem cells in response to injury (Raymond et al. 2006). In the brain, radial glia are present in periventricular zones (PVZ), which remain neurogenically active beyond postembryonic development (Raymond et al. 2006; Lindsey et al. 2012). In order to maintain neural stem cell populations, these cells must retain multipotency and self-renewal capacity, and prevent premature differentiation. While the regulation of stem cell identity has been widely studied in the context of intercellular signaling (e.g., Borday et al. 2012), newer perspectives on the molecular regulation of stem cells, including chromatin remodeling and pre-mRNA processing (Li et al. 2007; Mitrousis et al. 2015), are also being actively explored. My current research is specifically focused on the role of transcriptional and post-transcriptional regulation of stem cell function in the larval zebrafish retina and brain.

1.1. Stem cell niches in the zebrafish retina and brain

Early development of the vertebrate eye is fairly conserved across species (Fischer et al. 2013). The zebrafish eye is derived from the optic vesicles, evaginations of the diencephalon which

grow outward toward the surface ectoderm, whereupon the ectoderm thickens and invaginates to form the lens placode and ultimately the lens (Adler and Canto-Soler 2007). The optic vesicle also invaginates to form an optic cup with two distinct layers: 1) the internal layer, called the neural retina (NR), and 2) the external layer, called the retinal pigmented epithelium (RPE) (Adler and Canto-Soler 2007). During development, the NR gives rise to 6 distinct neuron types and 1 glia type which laminate into three layers: 1) the outer nuclear layer (ONL), which contains the cone and rod photoreceptors; 2) the inner nuclear layer (INL), which contains the horizontal cells, bipolar cells, and amacrine cells; and 3) the ganglion cell layer (GCL) (Livesey and Cepko 2001; Cayouette et al. 2006). The cell bodies of the retinal radial glia, known as Müller glia, are located within the INL, and the Müller glia have processes which extend the full apicobasal length of the retina (Lenkowski and Raymond 2014). Each cell type is generated from a pool of multipotent retinal progenitor cells which initially make up the NR after the optic cup is formed, around 24 hours post-fertilization (hpf) (Bassett and Wallace 2012). Differentiation of neurons in the eye begins centrally and radiates outward, eventually restricting the retinal progenitor cell population to the peripherally located CMZ (Raymond et al. 2006). A small population of self-renewing, multipotent retinal stem cells are located at the far periphery of the retina (Figure 2.1). Retinal stem cells will characteristically co-express eye-field transcription factors including *pax6*, *rx1*, and *vsx2* (Livesey and Cepko 2001; Raymond et al. 2006). These contribute to an adjacent population of the more committed retinal progenitor cells that eventually give rise to the various differentiated neurons (Fischer et al. 2013; Wan et al. 2016). By 60 hpf, embryogenesis of the zebrafish eye is complete and nearly all further growth of the eye during postembryonic development is due to neurons added from the CMZ (Wehman et al. 2005; Raymond et al. 2006). An exception is the addition of new rod photoreceptors, which arise sat a low frequency from Müller glia

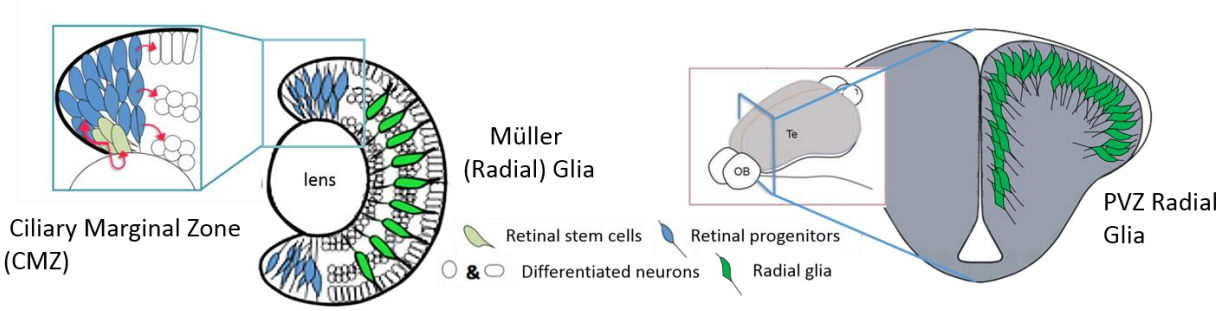

Figure 2.1 *Neurogenic niches are maintained in the zebrafish retina and brain.*
The ciliary marginal zone (CMZ) is located at the far periphery of the retina and contains a small population of self-renewing retinal stem cells, providing a constant source of retinal progenitor cells that can then differentiate into more specific cell types. Retinal radial glia (Muller glia) are distributed across the central retina, and occasionally dedifferentiate and proliferate to contribute to the rod photoreceptor population. Radial glia in the forebrain line the periventricular zone (PVZ) and similarly occasionally contribute to the neurons of the brain.

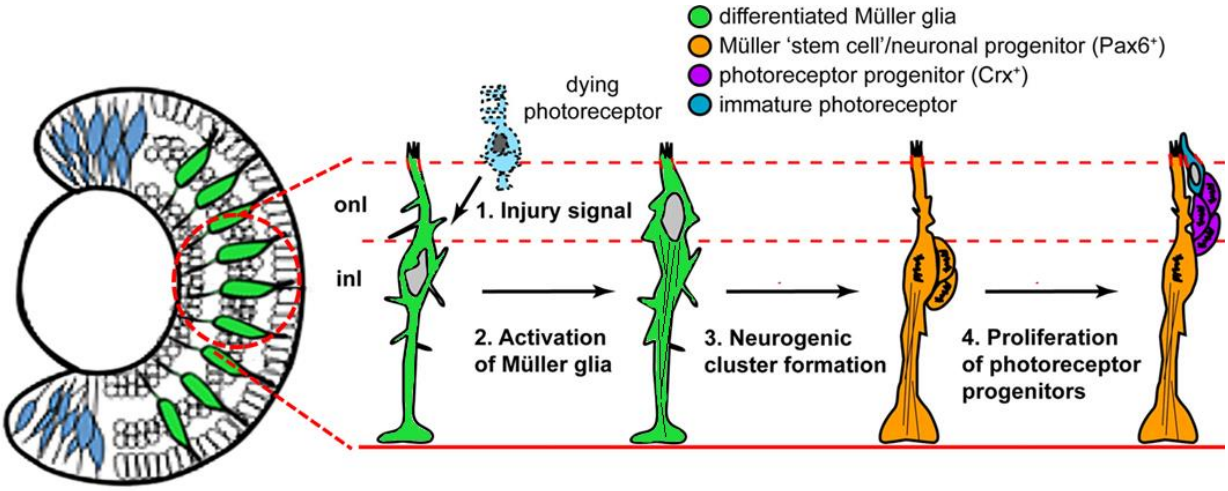

Figure 2.2 *Model of Muller glia-based photoreceptor regeneration in the adult zebrafish retina.*
Muller glia undergo dedifferentiation and rapid proliferation in response to retinal injury. This involves transient upregulation of stem/progenitor cell markers and a single asymmetric division which gives rise to a rod progenitor daughter cell. Figure adapted from Qin et al. 2009.

(Bernardos et al. 2007; Stenkamp 2011). Prior to reentering the cell cycle, Müller glia transiently upregulate genes associated with retinal stem cells (eg. *pax6, vsx2, rx1*); however, they still maintain glial identity as observed through maintained expression of glial-specific markers and cell morphology (Raymond et al. 2006; Lenkowski and Raymond 2014). In the non-injured retina, these partially dedifferentiated Müller glia will undergo a single asymmetric division resulting in a Müller glial daughter cell and a rod progenitor daughter cell. The newly born progenitor cell then migrates apically along the Müller glial processes to the ONL and contributes to the rod population (Bernardos et al. 2007). The neurogenic niche formed by the close association of the dividing Müller glia and its daughter cell shares many features in common with the CMZ as well as neurogenic niches found in the brain.

In the developing zebrafish forebrain, the telencephalon everts during morphogenesis resulting in the formation of a central T-shaped ventricle (Folgueira et al. 2012). Neurogenic niches containing radial glia are found in the area adjacent to the ventricle, known as the periventricular zone (PVZ) (Lindsey et al. 2012; Figure 1.1). As in the retina, radial glia of the PVZ act as stem cells which in the uninjured brain slowly divide and generate new neurons (Rothenaigner et al. 2011).

In the postembryonic zebrafish, individual radial glia in the retina and brain are relatively quiescent, only occasionally reentering the cell cycle; however, radial glial cells exhibit a robust proliferative response to injury (Figure 2.2). While Müller glia-derived progenitors are normally restricted to the rod lineage, regeneration assays have demonstrated that Müller glia are able to replenish any of the retinal neuron types (Fausett and Goldman 2006; Bernardos et al. 2007; Ramachandran, Reifler, et al. 2010). In the brain, normally quiescent radial glia of the PVZ are

activated in response to injury, proliferating and generating new neurons which migrate to the injury site (Kroehne et al. 2011; Barbosa et al. 2015).

1.2. Postembryonic regulation of neurogenic niches

Maintenance of neurogenic niches requires neural stem cells to retain self-renewal and multipotency properties as well as prevent premature differentiation. Proliferation and differentiation of stem cells must be tightly coordinated to ensure tissues are generated correctly and in synchrony with other developmental events.

Intercellular signaling is among the most widely studied molecular mechanisms implicated in regulating stem cell specification and maintenance. For instance, Hedgehog (Hh) signaling appears to be key in regulating the size of the retinal progenitor pool in the CMZ. Zebrafish larvae mutant for *patched2*, which causes overactive Hh signaling, exhibit postembryonic expansion of the CMZ through an increase in the number of progenitor cells (Bibliowicz and Gross 2009). Interestingly, the central retina of the *patched2* mutant is normal except for an underrepresentation of Müller glia (Bibliowicz and Gross 2009). Similarly, Wnt/β-catenin signaling has been implicated in regulating retinal stem cell identity. A study of *adenomatous polyposis coli* (*apc*) mutant zebrafish, which constitutively upregulate Wnt/β-catenin signaling, show early expansion of the CMZ accompanied by a central shift in the expression of retinal identity genes *sox2* and *atoh7* and a decrease in cell proliferation to rates characteristic of stem cells (Stephens et al. 2010). Activated Notch signaling is a hallmark of neural stem cells and in part contributes to the maintenance of the neurogenic niche. For instance, in dividing radial glia of the zebrafish PVZ, the daughter progenitor cell differentially inherits higher levels of Notch ligands, whereas its self-renewing counterpart displays higher Notch activity (Dong et al. 2012). Knockdown of the Notch ligand *dla* within radial glia clones transplanted to a wild-type host embryo was sufficient to bias

clones toward differentiation regardless of the presence of *dla* from surrounding wild-type cells (Dong et al. 2012). This suggests that not only is high Notch activity essential for maintaining self-renewal, but the balance of Notch signaling from within a single cell lineage is integral to maintaining the neurogenic niche.

Spliceosome dynamics and pre-mRNA processing have been implicated as critical features of stem cell regulation and survival. Genes involved in RNA processing and splicing have been shown to be activated during somatic cell reprogramming (Hirsch et al. 2015). Splicing patterns of stem cells are distinct from differentiated cells, and this is thought to be involved in maintaining multipotency (Hirsch et al. 2015). One mechanism of splicing regulation is governed by introns. In addition to the highly expressed major spliceosome, there is a second, minor spliceosome with more specialized utility (König et al. 2007). The minor spliceosome targets a rare class of introns which are highly conserved in genes involved in DNA repair, replication, transcription, RNA processing, and translation (Patel and Steitz 2003). Knockdown of minor spliceosome function in zebrafish embryos causes major developmental delays and leads to a decrease in cells detected in M-phase and S-phase coupled with an increase in apoptosis (König et al. 2007). It is therefore thought that the minor spliceosome is crucial for continually processing specific genes during cell proliferation. Given that neural stem cells retain proliferative capacity, they may have unique splicing requirements to maintain their identity.

Splicing is also regulated by the formation of the spliceosome, which is dependent on the availability of spliceosome components. The major spliceosome complex is formed from five essential small nuclear ribonucleoproteins (snRNPs): U1, U2, U4, U5, and U6, each of which houses a corresponding small nuclear RNA (snRNA) transcript (Strzelecka et al. 2010). snRNAs are intronless, non-polyadenylated RNA molecules usually between 100-200bp in length and are

responsible for intron/exon junction recognition and spliceosomal catalysis (Valadkhan 2010; Matera and Wang 2014). Transcription of snRNAs occurs in the Cajal body, a subnuclear compartment uniquely marked by the protein coilin (Machyna et al. 2013). Knockdown of coilin in zebrafish embryos leads to Cajal body disintegration and lethal disruption of cell proliferation, suggesting that coilin serves to concentrate spliceosome components in order to overcome rate-limiting assembly steps (Strzelecka et al. 2010). Recycling of spliceosome components is another way in which cells overcome rate-limiting steps. The zebrafish *earl grey* mutant, which has a lethal mutation mapped to the *p110* U4/U6 snRNP recycling factor, demonstrates defects in highly proliferative tissues including the eyes and brain (Trede et al. 2007). Expression profiling of the *earl* grey mutant revealed upregulation of genes associated with splicing and snRNP biosynthesis, suggestive of a compensatory mechanism to attempt to rescue the splicing defect. Of the genes affected by the lack of *p110*, the gene *kiaa0947l*, also called *ice1*, was the most highly up-regulated transcript (Trede et al. 2007).

1.3. The role of *ice1* in RNA Pol II-dependent snRNA transcription

RNA Pol II-dependent transcription requires the coordination of many factors to help recruit RNA Pol II to gene promoters and to promote elongation of transcription along the gene. Many protein-coding genes require the super elongation complex (SEC) for proper transcription. The SEC contains a number of factors including P-TEFb (positive transcription elongation factor) and *eleven-nineteen lysine-rich leukemia* (ELL) which act together to promote stable transcription elongation (Luo et al. 2012). In mouse embryonic stem cells, the SEC is essential for rapid transcriptional induction which allows genes to respond dynamically to developmental signals (Lin et al. 2011). An analogous ELL-containing complex specific to RNA Pol II- transcribed snRNA genes, called the little elongation complex (LEC), was identified in mammalian and *Drosophila*

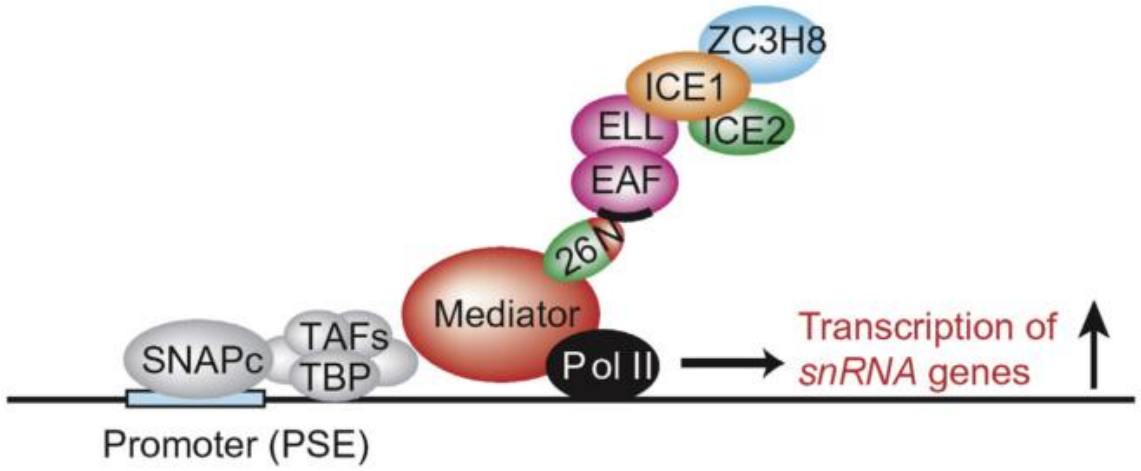

Figure 2.3 *Model of the little elongation complex (LEC) recruitment of RNA Polymerase II to initiate snRNA transcription.*
The LEC core component is ICE1, which acts as a scaffold for several proteins including ICE2, ZC3H8, and ELL. SNAPc bound to the proximal sequencing element (PSE) upstream of the 3' box of snRNA promoters recruits the Mediator 26 complex and the LEC, which allows RNA Polymerase II recruitment and initiation of snRNA transcription. Figure taken from Anwar et al. 2016.

cells *in vitro* (Smith et al. 2011;Figure 1.3). The LEC contains ELL-associated factors (EAFs), and two interactors of the carboxy-terminus of ELL, called ICE1 and ICE2 (Takahashi et al. 2015).

Knockdown studies in mammalian cell culture show that ICE1 is required for snRNA transcription by recruiting RNA Pol II to snRNA gene promoters (Hu et al. 2013). In contrast, knockdown of ELL in the same study did not appear to affect RNA Pol II occupancy at promoters, but elongation of snRNA transcription was inhibited (Hu et al. 2013). Loss of recruitment of the entire LEC complex at snRNA genes leads to an overall reduction in snRNA transcription (Takahashi et al. 2015). Similarly, repressing LEC formation by inhibiting ELL-ICE1 interaction through overexpression of p53, a known interactor of ELL, is sufficient to reduce snRNA transcription (Anwar et al. 2016). Therefore, ICE1 is thought to be an essential LEC scaffolding component required for snRNA transcription. The zebrafish *ice1* is orthologous to the human and mouse *ICE1* genes (Sprague 2006). However, all studies to date on the LEC and its components have only been conducted under *in vitro* conditions in cell lines.

1.4. An *in vivo* loss-of-function model for *ice1*

Recently, the *kes*^{s546} mutant, discovered by the Baier lab in a zebrafish ENU mutagenesis screen searching for postembryonic CMZ defects (Wehman et al. 2005), was mapped by our lab to the *ice1* locus (Figure 2.4). The *kes*^{s546} mutant contains a single base pair nonsense mutation (C→T) in exon 15 of the *ice1* gene. This results in a predicted premature stop codon, which would prevent translation of the ICE1 C-terminus. Takahashi et al. (2015) demonstrated through deletion mutants that the C-terminal fragment of ICE1 (1,191-2,266) is essential for interaction with ELL and is itself sufficient for the formation of the LEC. Thus, it can be reasonably expected that cells in the *ice1* mutant would exhibit repressed LEC formation and therefore reduced snRNA transcription.

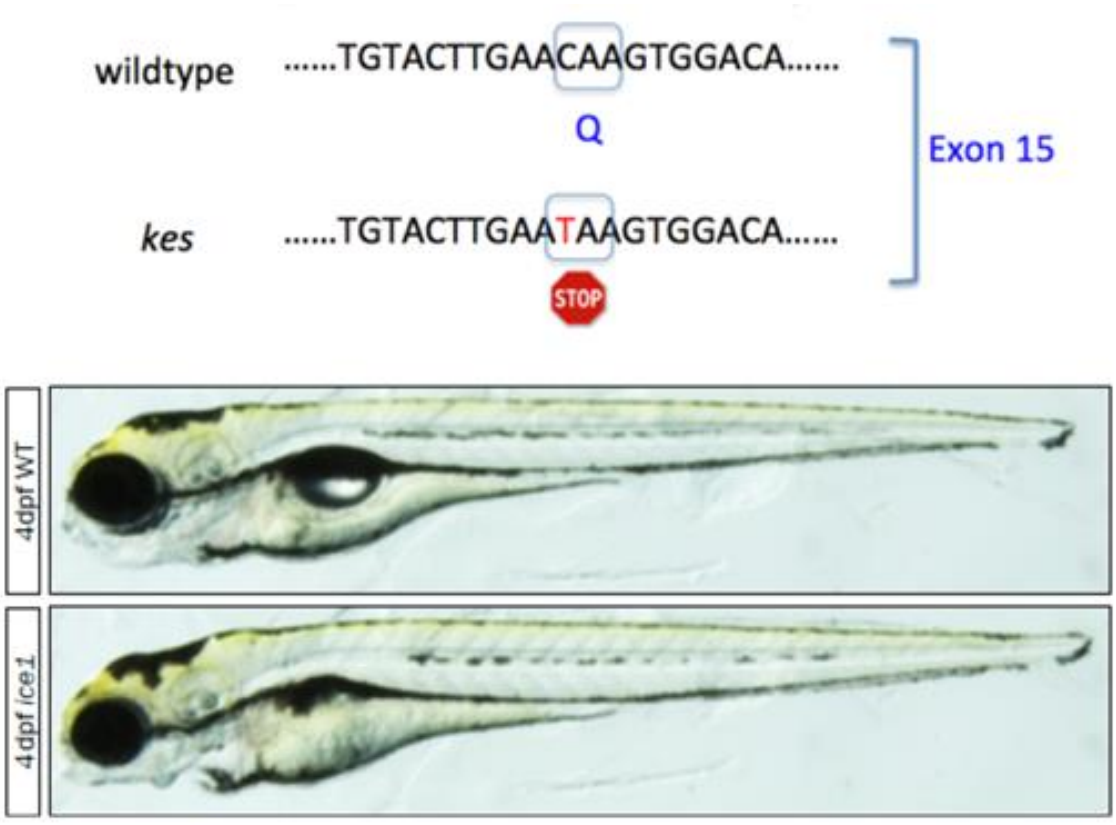

Figure 2.4 *The ice1 mutant contains a putative premature stop codon in exon 15.*
The *kes* mutant discovered in the Baier lab was mapped to the *ice1* locus, which results in a premature stop codon abolishing much of the ice1 protein C-terminus. *Ice1* mutants exhibit a small eye, small brain phenotype visible at 4dpf. Figure taken from Sorfazlian 2015.

The *ice1* mutant exhibits small eye morphology (microphthalmia), reduced CMZ and expanded peripheral retinal pigmented epithelium (RPE) at 4dpf (Wehman et al. 2005). Cell cycle marker analysis showed that mutant CMZ cells appear to be arrested in the G1 cell cycle stage and removed by apoptosis, therefore unable to continually renew the retinal stem cell pool (Sorfazlian 2015). Despite these severe phenotypes, eye development appears to progress normally up until the 4dpf stage.

Quantitative PCR results show high maternally contributed *ice1* expression at 1hpf and 4hpf, with expression dropping significantly by 1dpf. *In situ* hybridization demonstrates global *ice1* expression within 1dpf, whereas beyond 1dpf the expression becomes restricted to the head including the retina and brain tissues (Sorfazlian 2015). This suggests that the maternal contribution of *ice1* is able to rescue the mutant until zygotic transcription would normally take over, resulting in the delayed phenotype onset. *Ice1*-morpholino knockdown in single-cell embryos results in similar morphant phenotypes visible at 1dpf, including decreased head and eye development, further suggesting that *ice1* expression is required for early development (Sorfazlian 2015).

Chapter 2
Aims and Hypothesis

Currently, there are no *in vivo* models of *ice1* function. Moreover, the relative homogeneity of immortalized cell lines precludes analyses of cell type specific functions in developing tissues. *Ice1* has been shown to be required for both RNA Pol II recruitment at snRNA gene promoters, and for transcription elongation of snRNA genes; however, its role in the transcription of other genes has not yet been studied. Though preliminary data (Sorfazlian 2015) indicate that *ice1* expression becomes restricted to the eyes and brain by 3dpf, the cell type-specificity of *ice1* expression and how it might change over time has not yet been assayed. Finally, whether *ice1*-dependent snRNA gene expression is differentially required in stem cells (active or relatively quiescent) versus differentiated cells *in vivo* has not been tested.

Based on these previous studies, **I hypothesize that the zebrafish *ice1* mutant has reduced snRNA gene expression and overall decreased splicing efficiency, which predominantly affects the maintenance of neural stem cell populations in the brain as well as the retina.** To test my hypothesis, I have addressed three research aims: 1) to characterize the phenotype of *ice1* mutant neural stem cells in the brain and retina; 2) to examine the impact of *ice1* deficiency on transcript levels in isolated neural stem cells; and 3) to investigate the importance of *ice1* in the context of regeneration.

Neural stem cells can be constitutively active, as in the CMZ, or relatively quiescent, as in radial glia populations. To investigate the effect of *ice1* deficiency in different stem cell populations, I performed an immunohistochemical characterization of neural stem cell compartments in the retina and forebrain of the *ice1* mutant. The resulting data provides insight

into a possible link between active cell proliferation and sensitivity to splicing defects in neural stem cells.

The CMZ stem cell population is mostly abolished in *ice1* mutants by 4dpf; however, radial glia in the retina and forebrain are still retained. I have created a transgenic radial-glia fluorescent reporter line crossed into the *ice1* mutant background, which has allowed me to successfully isolate radial glia for gene expression profiling. I believe the resulting data provides new insight into how *ice1* regulates gene expression in postembryonic stem cells and differentiated neural cells.

Normally quiescent Müller glial cells respond to retinal injury by partially dedifferentiating into an active stem cell state. The regeneration response involves transient upregulation of stem cell markers followed by a round of asymmetric division to generate a new progenitor cell. To determine the importance of *ice1* in the context of regeneration, I examined the effect of UV retinal lesion on the dedifferentiation response in the *ice1* mutant. The results illuminate the potential role of *ice1* in a stem cell type, which can be both quiescent and active.

Chapter 3
Materials and Methods

3.1. Zebrafish Maintenance and Husbandry

Adult zebrafish (*Danio rerio*) were raised and bred at 28˚C on a 14 hour light/10 hour dark cycle. All zebrafish used in this study were treated in accordance with regulations on animal experimentation as established by the Canadian Council on Animal Care. Maintenance, breeding, and experimental procedures were approved by the University of Toronto Animal Care Committee. Embryos were staged as described in Kimmel et al. (1995) and reared according to standard procedures (Westerfield 2007). The wild type strain used was AB received from the Zebrafish International Resource Centre (ZIRC). The mutant strain used was *kes*^{s564} (*ice1*) received from Dr. Herwig Baier (Max Planck Institute of Neurobiology, Germany). The radial glia reporter strain used was *Tg(her4.1:mCherryT2ACreERT)* [referred to as *Tg(her4.1:mCherry)* throughout this thesis], which was generated by Dr. Zachary Hall, a postdoctoral fellow from our lab, and the *Tg(GFAP:GFP)* radial glial reporter line was generously provided by Dr. Pierre Drapeau (Université de Montreal). Adult *ice1* heterozygotes were bred with *Tg(her4.1:mCherry*) fish and larvae were visually inspected for mCherry fluorescence after 2-3 days post fertilization (dpf) before raising to adulthood. Adult carriers of the *ice1* mutant allele were identified by Sanger sequencing (The Centre for Applied Genomics, University of Toronto). Primers used for genotyping are: ice1-seq-F (TCCCATGACCCAGTGAATCTG), ice1-seq-R (TCTCTTTGGGCAGTGCTTGA). *Ice1* sibling refers to a mixture of larvae with *ice1*$^{+/+}$ and *ice1*$^{+/-}$ genotypes from a pooled clutch, whereas *ice1* mutant refers to larvae with *ice1*$^{-/-}$ genotype from the same pooled clutch.

3.2. Immunohistochemistry

Larvae were fixed in 4% paraformaldehyde overnight at 4˚C and dehydrated in a sucrose series for cryoprotection. Samples were processed at -20˚C into 20µm sections using a cryostat (Leica). Cryosections were then rehydrated with PBS and blocked for minimum 1 hour in 0.2% Triton X-100 + 2% goat serum in PBS at room temperature (RT). Primary antibodies in block solution were applied to sections and incubated overnight at 4˚C. Sections were then washed in PBS + 0.1% Tween-20 and incubated with secondary antibodies (1:200 Cy2, 1:500 Cy3/Cy5, Jackson ImmunoResearch Laboratories, Inc.) for minimum 2 hours at RT. Nuclei were stained with 10µg/mL Hoechst before mounting slides in glycerol. All primary antibodies used and their concentrations are listed in Table 3-1. Images were taken with Leica TCS SP8 confocal microscope and analyzed with Leica LAS AF software and ImageJ.

3.3. Cell Counting Analysis

Cell counts were performed using Imaris software (Bitplane). Masked 3D representations of confocal image stacks were created for each region of interest (CMZ, central retina, forebrain). Regions were manually traced using anatomical markers: CMZ was defined as periphery of the retina up to the beginning of the INL/ONL laminations; central retina was defined as the outline of the retina excluding the CMZ defined region; the entire forebrain region was used for counts. Intensity threshold for each surface object was adjusted to best match the original image. Parameters based on cell morphology, size, and intensity were used to detect cells. Average cell counts were taken over two consecutive sections for at least four biological replicates. Counts were taken as absolute cell counts per section (CMZ) or normalized to Hoechst (central retina and forebrain) and statistical differences ($p < 0.05$) were determined by Student's t-test (Graphpad Prism).

3.4. Fluorescence Activated Cell Sorting (FACS) of Radial Glia Cells

4dpf *ice1*;*Tg(her4.1:mCherry)* larvae, or *Tg(GFAP:GFP)* larvae, were visually identified as siblings or mutants and whole heads (n=30-40 per group) were dissected on ice. Heads were dissociated in papain enzyme (Worthington Biochemical, NJ) for 20-25 minutes at 37˚C and gently manually triturated. Dissociated cells were pelleted and resuspended in 10% fetal bovine serum (FBS) + 30nM DAPI + 1mM EDTA + 25nM HEPES in phosphate-buffered saline (PBS). FACS was performed on live cells at 17psi/100µm nozzle on a BD Influx (Faculty of Medicine Flow Cytometry Unit, University of Toronto). Cells were sorted by size and DAPI-exclusion to ensure only single, viable cells were collected. mCherry positive and negative cells for each group were collected directly into TRIzol and standardized by volume to equal cell number inputs per sample. RNA extraction of samples was performed immediately following FACS.

3.5. RNA extraction and cDNA synthesis

Total RNA was extracted from an equal amount of sorted cell samples using TRIzol reagent (Life Technologies) as per the manufacturer's protocols. Residual DNA in RNA samples was digested with TURBO DNase (Life Technologies) at 37˚C for 30 minutes. RNA was precipitated in isopropanol in the presence of glycogen and resuspended in RNase-free water. cDNA was synthesized from RNA using SuperScript III Reverse Transcriptase (Life Technologies) and mixed random/oligo-dT primers as per the manufacturer's instructions.

3.6. RNA-sequencing (RNA-seq) and Analysis

RNA-seq library was generated from whole 4dpf *ice1* sibling and mutant heads collected and extracted by Natalie Sorfazlian. Total RNA was extracted by TRIzol as described in section 3.5 and RNA was subsequently re-purified by phenol-chloroform extraction. RNA sequencing and

analysis was conducted at The Centre for Applied Genomics (TCAG) at the Hospital for Sick Children. RNA quality was assessed by Agilent Bioanalyzer 2100 RNA Nanochip before proceeding with cDNA library preparation using the Illumina TruSeq Stranded Total RNA Library Prep Kit. 400ng of RNA was used per sample, and ribosomal RNAs were depleted using RiboZero Gold. Library fragments were amplified under the following conditions: 98˚C, 10s; 14x (98˚C, 10s); 60˚C, 30s; 72˚C, 30s; 72˚C, 5min. Paired-end sequencing was performed on an Illumina HiSeq 2500 platform on High Throughput run mode flowcell and V4 sequencing chemistry. The reference genome used was danRER7 (Zv9) and analysis was performed using Cufflinks. Read counts for gene expression were input into edgeR (Bioconductor) for differential expression analysis performed. Gene expression, intron retention, and 3'UTR retention analysis was performed in collaboration with Dr. Yunchen Gong, a bioinformatics specialist at the Centre for the Analysis of Genome Evolution & Function (University of Toronto).

3.7. Real-time Quantitative PCR (RT-qPCR)

RT-qPCR was performed using a CFX384 Touch™ Real-Time PCR Detection System (Bio-Rad; generously loaned by Dr. Jennifer Mitchell). PCR conditions were as follows: 95˚C, 5min; 40x (94˚C, 1min; 58˚C, 30s; 72˚C, 30s); 72˚C, 10min. Primer sequences are listed in Table 3.2. All samples were run in triplicate for experimental replicates and in triplicate for biological replicates. Statistical significance ($p < 0.05$) between groups was assessed using repeated measures one way ANOVA and Tukey post-hoc multiple comparisons (Graphpad Prism).

3.8. UV Lesion and EdU Incorporation Assay

4dpf *ice1*;*Tg(her4.1:mCherry)* sibling and mutant larvae were anaesthetized in Tricaine and embedded in 0.5% agarose on their sides. Larvae were exposed to UV light (405nm) under a compound microscope (Leica) equipped with a discharge lamp (Kubler, Hofstra Group) at

maximum intensity for 40 minutes, removed from the agarose, and returned to facility water to recover overnight. At 24 hours post lesion (hpl), larvae were treated with 5mM EdU for a 6 hour pulse and immediately sacrificed. Larvae were fixed in 4% paraformaldehyde overnight at 4˚C and cryosectioned and processed as described in section 0. EdU was detected using the Click-It EdU Alexa Fluor 647 Imaging Kit (Life Technologies) according to manufacturer specifications.

3.9. Chromatin Immunoprecipitation (ChIP)

ChIP assays were performed on whole heads taken from 4dpf *ice1* mutants and siblings using the EZ ChIP kit (Millipore) as per the manufacturer's instructions. Tissue was crosslinked in 1% formaldehyde in PBS at RT for 15 minutes and quenched with 0.125M glycine. The samples were washed in PBS and incubated with protease inhibitor and SDS lysis buffer. Sonication was performed using Bioruptor (Diagenode) using 3 cycles at 30% power. Antibodies for RNA Pol II (Millipore) and mouse IgG negative control (Millipore) were used at 2µg per sample. 1% input was reserved from each sample to compare starting chromatin levels across samples. Gene expression was quantified by real time qPCR as described in section 3.7.

Table 3-1 *List of antibodies, concentrations, and sources.*
Sources include rabbit (Rb) and mouse (M).

Antibody (Source)	**Target**	**Conc. Used**	**Company**
PCNA (Rb)	Proliferative cell nuclear antigen	1:200	Sigma-Aldrich
GS (M)	Glutamine synthetase (radial glia)	1:200	Abcam
dsRed (Rb)	mCherry	1:500	Clontech
PHH3 (Rb)	Phosphohistone H3 (M-phase)	1:200	Cell Signaling
Caspase3 (Rb)	Caspase-3 (apoptosis)	1:200	Cell Signaling
Zpr1 (M)	Red/green cone photoreceptors	1:400	ZIRC
HuC/D	HuC/HuD proteins (differentiated neurons)	1:400	Molecular Probes
β-catenin (M)	Adherens junctions	1:200	BD Biosciences

Table 3-2 *Primer sequences used for RT-qPCR.*
Primer sequences were aligned with the zebrafish genome (GRCz10) using the UCSC Genome Browser. F = forward, R = reverse

Primer Name	**Sequence (5' → 3')**
18S-F	TCGCTAGTTGGCATCGTTTATG
18S-R	CGGAGGTTCGAAGACGATCA
glula-ex-F	GTGTGAAGGCATTGACATGG
glula-ex-R	CATCTTCCCGCATTTCCTTA
uspl1-ex-F	TGCCTTTACCCGTTGGTTAG
uspl1-ex-R	AGGGTGGCATCATTGACTTC
sart3-ex-F	GGAGGAGCTCATGGAGACAG
sart3-ex-R	TCCCACAACCCTGAAACAAT
U1-qPCR-F	CAATCGCGGCTTCTCGTTG
U1-qPCR-R	GAACGCAGTCCCCCACTAC
U2-qPCR-F	CTGATACGTGCCCTACCCG
U2-qPCR-R	ACTGCAATACCGGGTCGATG
U6-qPCR-F	GCTTGCTACGGTGGCACATA
U6-qPCR-R	TATGGAGCGCTTCACGGATT
U11-qPCR-F	AAAGGGCATCTGCTGTGAGT
U11-qPCR-R	AGCAGCCCCGTGTCATAAAA
p53-qPCR-F	ATCATCTGAGCCCAAACAGG
p53-qPCR-R	ACAAAGGTCCCAGTGGAGTG

Chapter 4

Results

4.1. Characterizing the mutant neural stem cell phenotype in the retina and forebrain

4.1.1. Cells in the *ice1* mutant CMZ exhibit cell cycle arrest and increased apoptosis

Previous work demonstrated that the constitutively active stem cells of the CMZ appear to undergo cell cycle arrest and are subsequently removed by apoptosis in the *ice1* mutant (Sorfazlian 2015). As previously described, *ice1* mutant CMZ cells at 4dpf are positive for PCNA, a marker of actively proliferating cells (Figure 4.1). Though these cells appear to be "proliferative", I found consistent reduction of cell cycle stage markers at this time point. EdU labeling, which denotes cells undergoing S-phase, was found to be abnormally absent in the mutant CMZ (Figure 4.2). Similarly, there was a significant decrease in mutant CMZ cells positive for phosphohistone H3 (PHH3), a marker of M-phase, compared with siblings (Student's t-test, $p < 0.05$) (Figure 4.3). On the other hand, the amount of apoptosis in the *ice1* mutant CMZ is much greater compared with the wild-type. A significant increase in the number of cells positive for caspase3, a marker of apoptosis, was found in the mutant CMZ (Student's t-test, $p < 0.05$) (Figure 4.4). This analysis confirms that in the CMZ constitutively active stem cell population, *ice1* is required for proper cell cycle progression and maintenance of neural stem cells.

4.1.2. The Müller glia of the central retina are relatively unaffected in the *ice1* mutant

The central retina houses postmitotic differentiated neurons and relatively quiescent Müller glia. As expected under normal circumstances, there is an absence of PCNA, PHH3, and EdU staining in the central retina of both the *ice1* siblings and mutants (Figure 4.1-Figure 4.4).

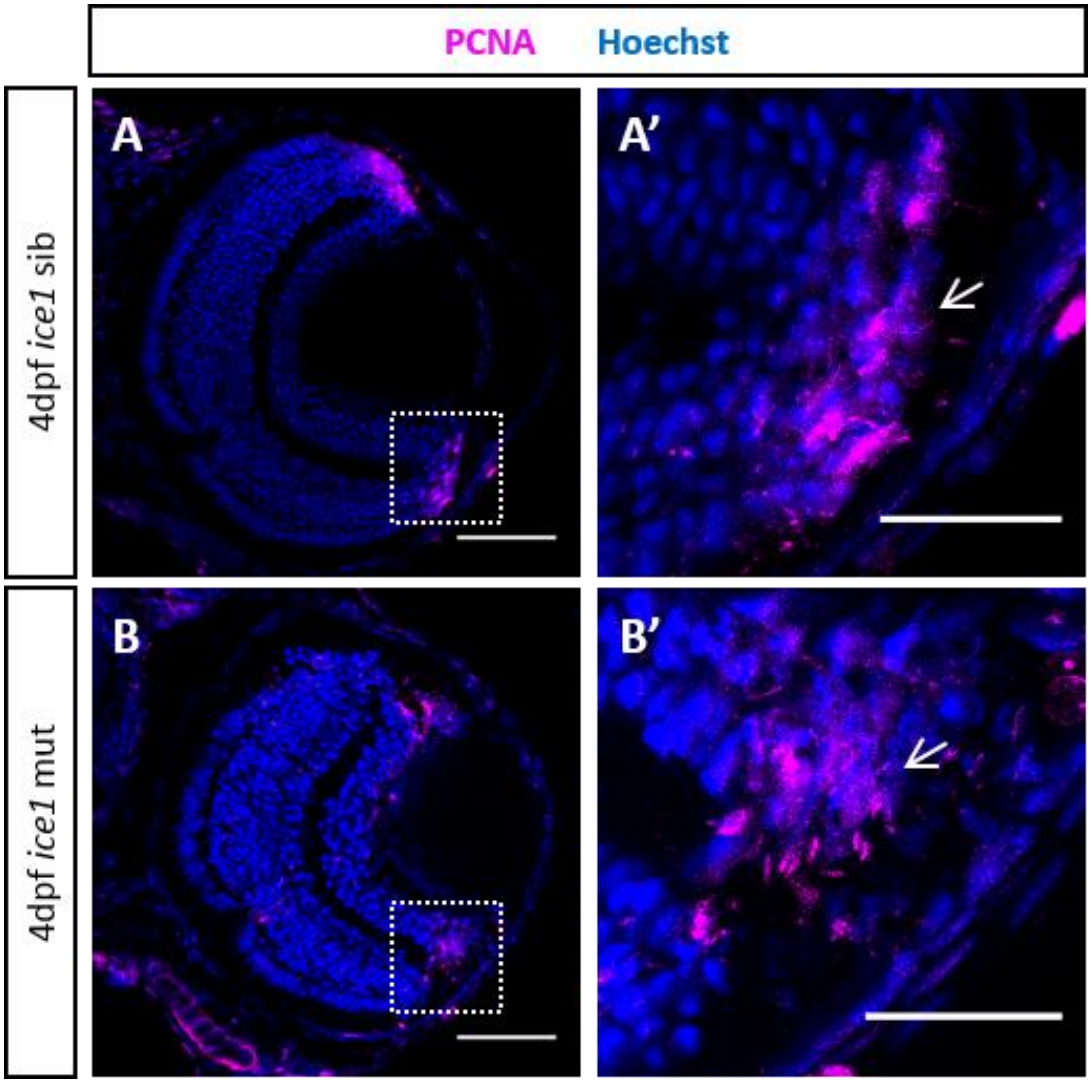

Figure 4.1 *The* ice1 *mutant CMZ appears to remain proliferative.*
Ice1 siblings normally do not express PCNA (magenta) in the central retina (A) but do exhibit PCNA labeling in the CMZ (A') at 4dpf. Comparable to siblings, no PCNA was detected in the *ice1* mutant central retina (B). Although the mutant CMZ is restricted, PCNA labeling was still observed (B'). Scale bar = 50µm (A, B); 20µm (A', B').

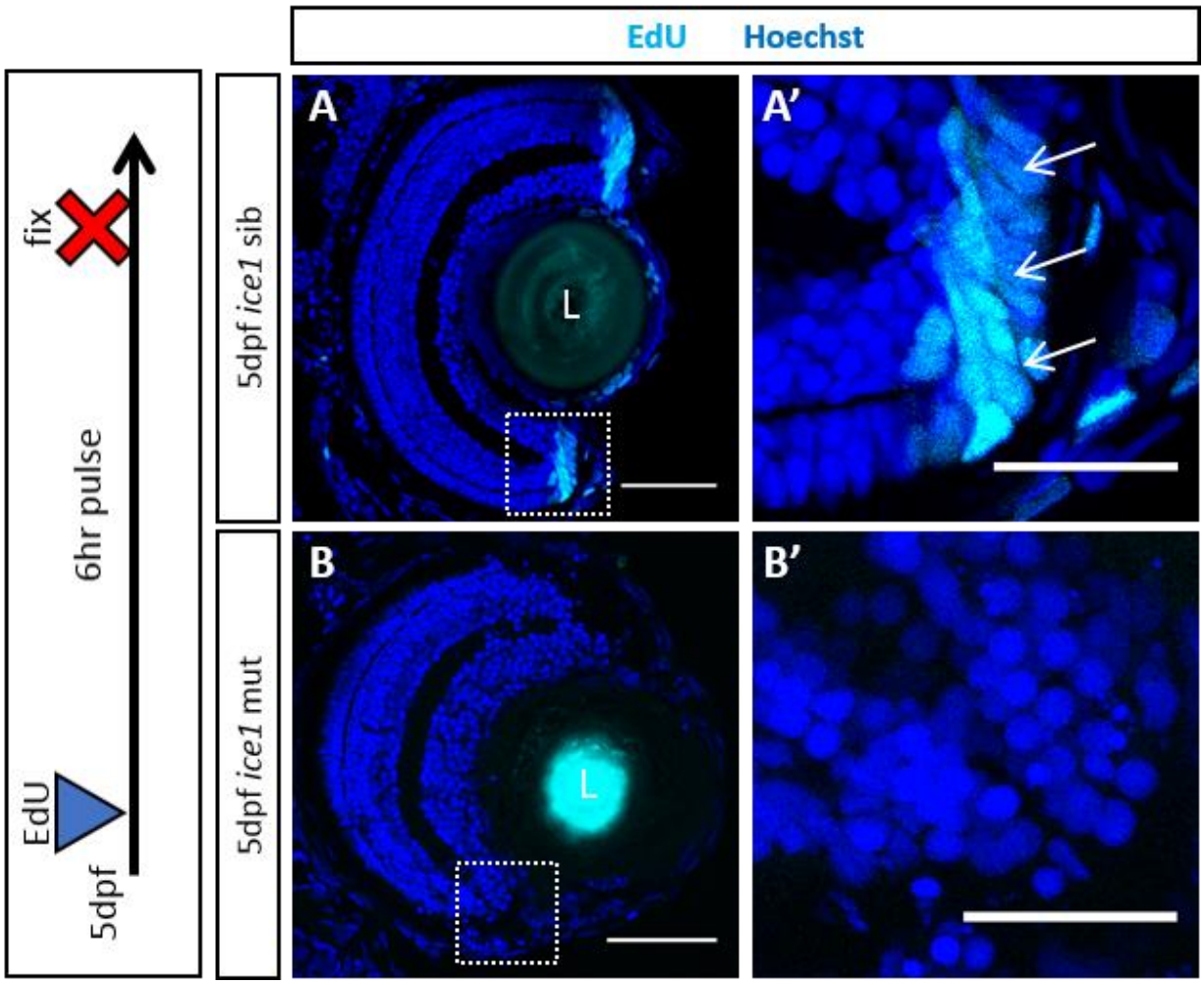

Figure 4.2 *No detection of cells undergoing S-phase after 6hr EdU pulse in the* ice1 *mutant CMZ. Ice1* siblings pulsed with EdU (in cyan) for 6hr at 5dpf show strong EdU labeling in the CMZ (A'), whereas EdU labeling in the *ice1* mutant CMZ is completely absent (B'). No EdU is detected in the central retina of *ice1* siblings (A) or mutants (B). L = lens, scale bar = 50µm (A, B); 20µm (A', B').

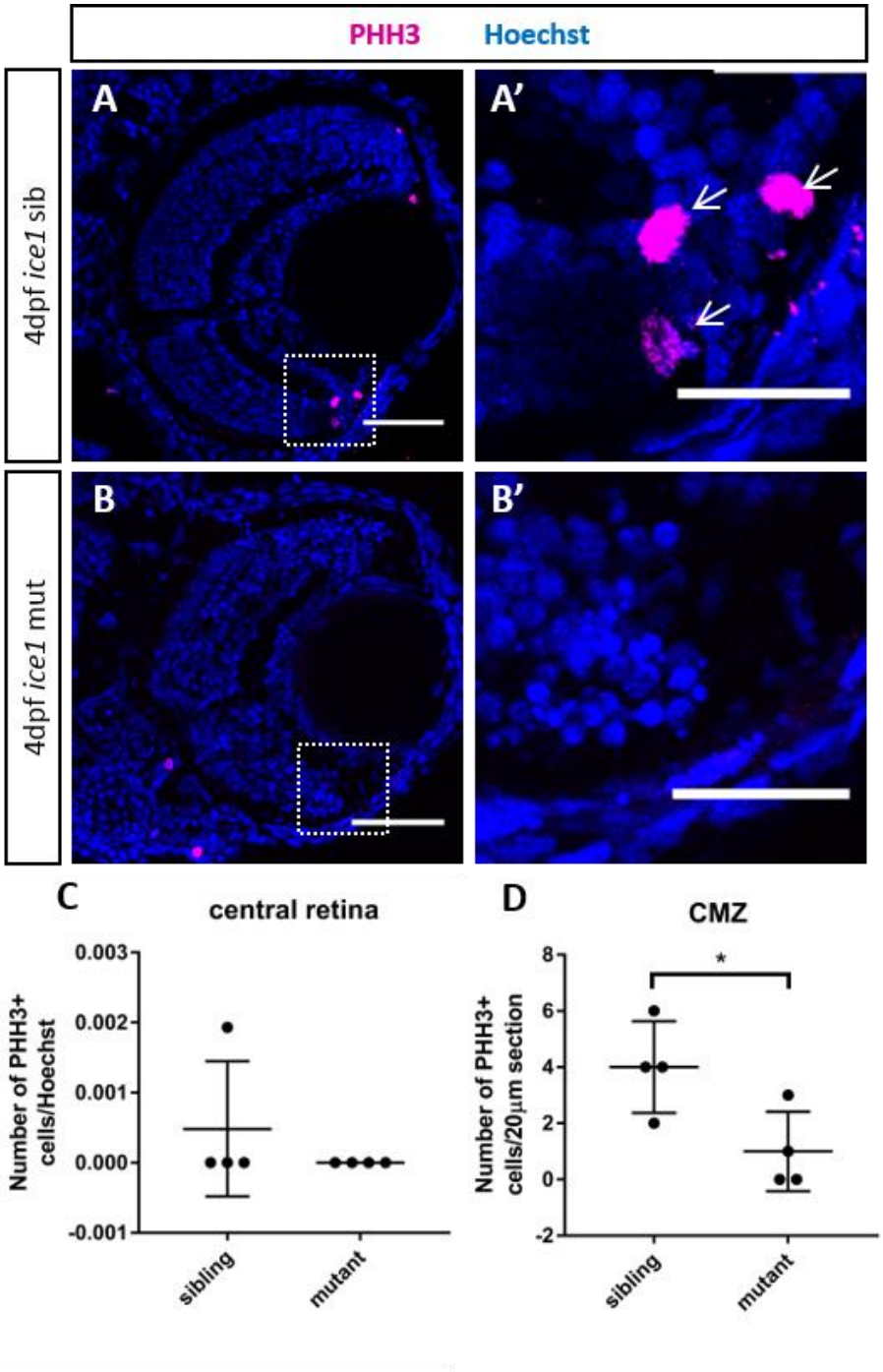

Figure 4.3 *Fewer cells undergoing mitosis in the* ice1 *mutant CMZ.*
Little to no detection of the mitosis marker PHH3 (in magenta) was observed in the central retina of *ice1* siblings (A) and mutants (B). Quantification of PHH3 levels in both groups demonstrated no significant differences (C). In contrast, the *ice1* sibling shows high levels of PHH3 in the CMZ (arrows, A'), whereas the *ice1* mutant CMZ shows little or no PHH3 expression (B'). Numbers of PHH3+ cells were quantified in both groups and were found to be significantly lower in the *ice1* mutant (D). Scale bar = 50µm (A, B); 20µm (A', B').

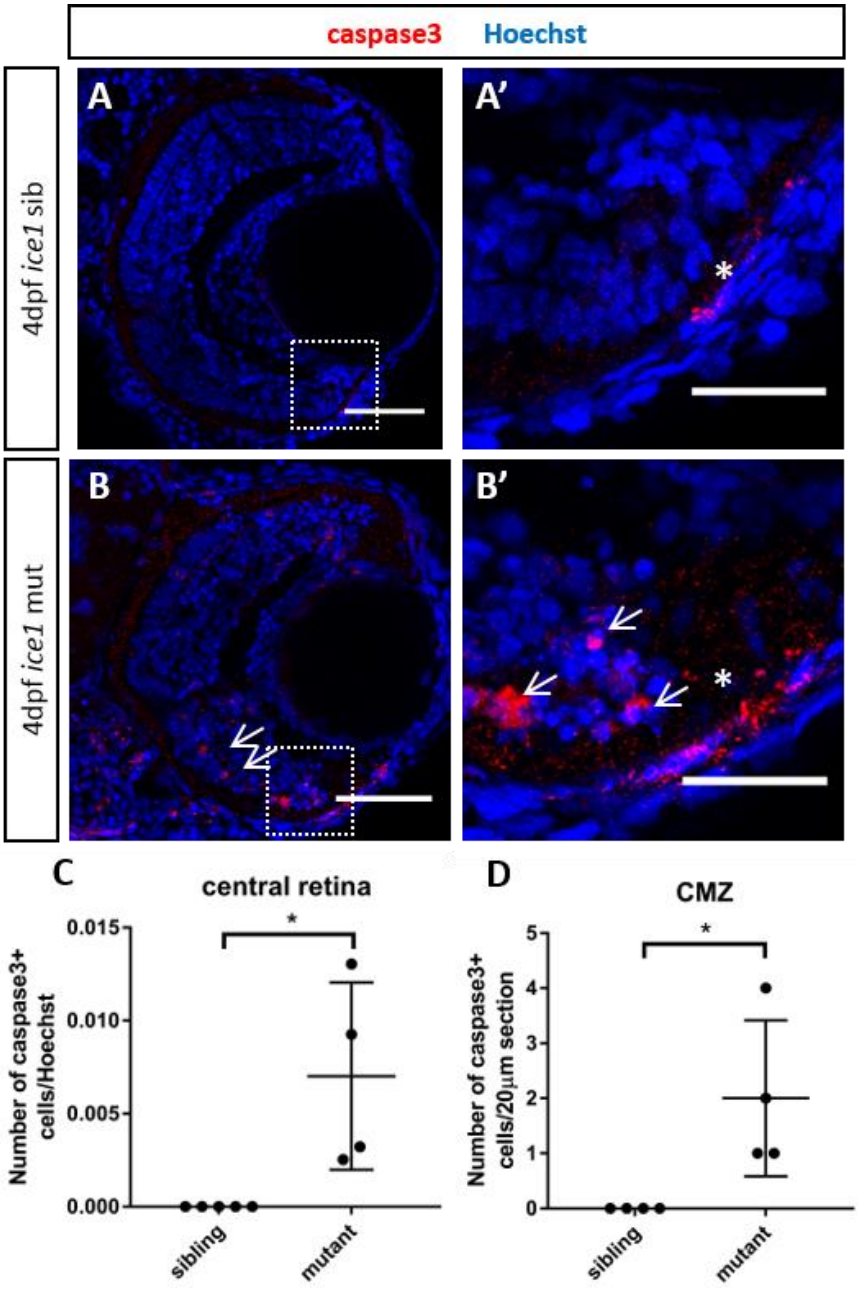

Figure 4.4 *Increased apoptosis in the CMZ and central retina of the* ice1 *mutant.*
There is little to no detection of the apoptosis marker caspase3 (in red) in the central retina (A) and the CMZ (A') of the *ice1* sibling. In contrast, *ice1* mutants exhibit numerous caspase3+ cells throughout the central retina (B, arrows) and the CMZ (B'). Caspase3+ cells were quantified in both groups and were found to be significantly higher in the central retina (C) and CMZ (D) of the *ice1* mutant in comparison to siblings. Arrows denote caspase3+ cells, asterisks denote nonspecific staining. Scale bar = 50µm (A, B); 20µm (A', B').

There is, however, a significant increase in caspase3+ cells in the mutant central retina (Student's t-test, $p < 0.01$). The apoptotic cells are observed in all three layers of the retina and this implies that dying cells are not specific to a particular neuronal subtype, although this would have to be confirmed by quantifying caspase3+ cells co-labeled with cell type specific markers. It is possible that the increased apoptosis in the central retina may be sufficient to induce a regenerative response in the wild type retina. Although the Müller glial cells appear unaffected in the *ice1* mutant, perhaps given the widespread increase in apoptosis the Müller glia are incapable of responding to injury to promote tissue repair. I later examined this possibility more thoroughly using a UV lesion protocol as described in section 3.8.

4.1.3. The *ice1* mutant PVZ radial glia exhibit similar cell cycle defects to the mutant CMZ

The radial glial cells in the PVZ of the forebrain represent a pool of relatively quiescent stem cells diving asynchronously. Although individual cells divide at a low frequency, the niche as a whole can be considered constitutively active. Based on the qualitatively smaller head and brain (microcephaly) and absence of *ccnd1* along the PVZ observed in the mutant (Sorfazlian 2015), the PVZ radial glial cells may respond to *ice1* deficiency in a similar manner as the mutant CMZ. It is important to note, however, that the stem cells in these two compartments have distinct characteristics. In the CMZ, stem cells do not express typical radial glial markers, such as GFAP or glutamine synthetase (Raymond et al. 2006). Using immunolabeling for cell cycle markers, I examined whether similar defective cell cycle features could be observed in the *ice1* mutant forebrain.

The *ice1* mutant PVZ remains PCNA-positive but is highly disorganized compared with the siblings. Whereas the PVZ normally forms a distinctive T-shape alongside the telencephalic

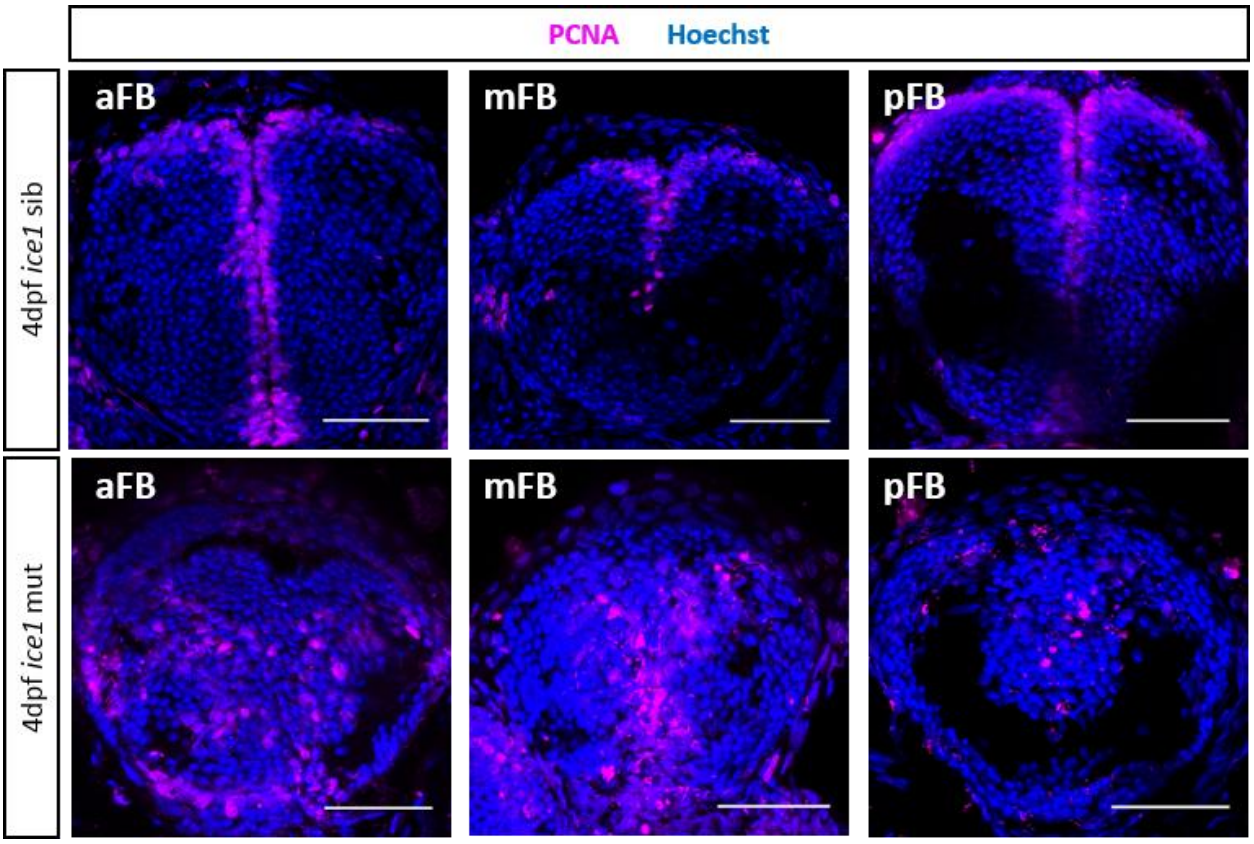

Figure 4.5 *The* ice1 *mutant PVZ appears morphologically compromised but proliferative.*
In the *ice1* sibling PVZ, PCNA staining is observed along a distinct single cell thick region adjacent to the forebrain ventricle. In contrast, the *ice1* mutant PVZ does not exhibit its distinctive morphology and PCNA staining is observed in what would normally be the differentiated zone. aFB = anterior forebrain, mFB = mid forebrain, pFB = posterior forebrain. Scale bar = 50µm.

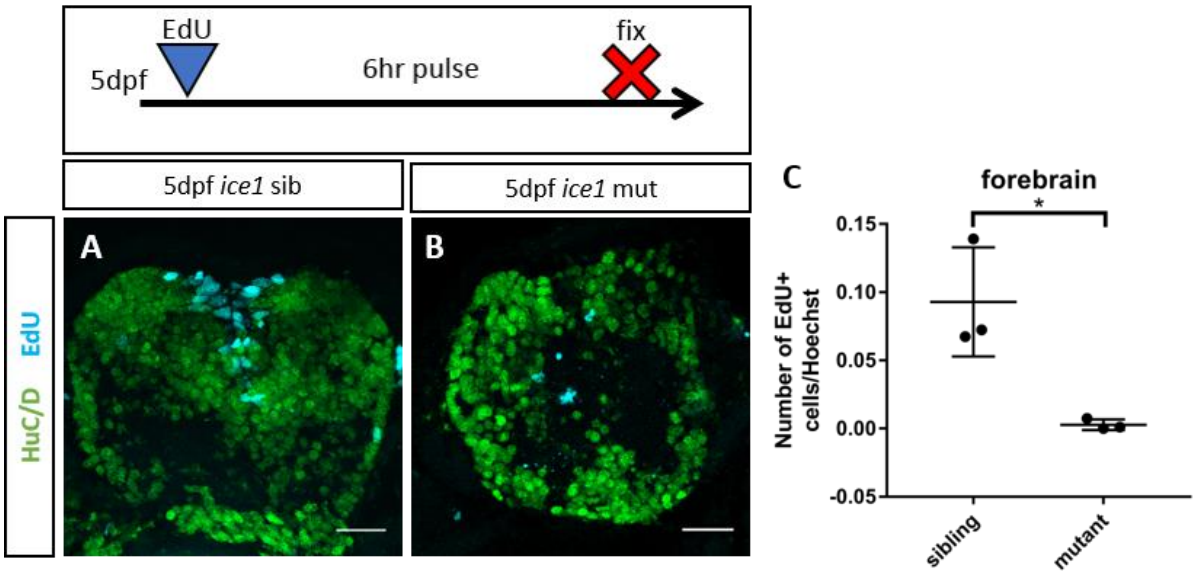

Figure 4.6 *Cells undergoing S-phase are greatly reduced in the* ice1 *mutant forebrain.*
Ice1 siblings pulsed with EdU (in cyan) for 6hr at 5dpf show strong EdU labeling along the PVZ, and staining for the differentiated neuron marker HuC/D (in green) does not co-label with EdU+ cells (A). Although the HuC/D staining pattern is similar in mutants, there are few EdU+ cells detected in the PVZ (B). Significantly fewer EdU+ cells were detected in *ice1* mutant forebrains compared with siblings (C). Scale bar = 20µm.

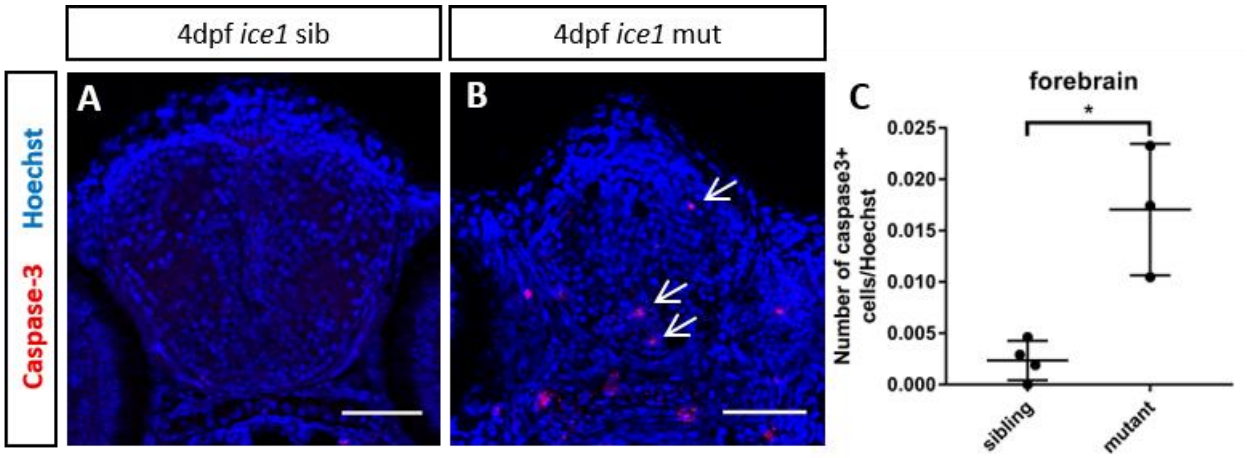

Figure 4.7 *Increased apoptosis in the* ice1 *mutant forebrain.*
There is little to no detection of the apoptosis marker caspase3 (in red) in *ice1* sibling forebrain, whereas caspase3+ cells are observed the *ice1* mutant (arrows). Caspase3+ cell counts were found to be significantly higher in the forebrain of the *ice1* mutant in comparison to siblings. Scale bar = 50µm.

ventricle, the structure of the mutant PVZ looks compromised and PCNA labeling appears more diffuse through the central forebrain (Figure 4.5). While EdU is normally detectable along the PVZ, it is greatly reduced in the *ice1* mutant PVZ (Figure 4.6).

Concomitant with the near absence of these cell cycle markers is a significant increase in the number of caspase3+ cells in the *ice1* mutant forebrain (Student's t-test, $p < 0.01$) (Figure 4.7). Thus, similar to the retinal stem cells of the CMZ, *ice1* deficiency appears to cause cell cycle progression defects in the mutant PVZ radial glia as demonstrated by reduced or absent expression of cell cycle markers. This appears to be coupled to cell cycle arrest and increased apoptosis in the forebrain suggesting that the radial glia within the PVZ niche is being progressively lost due to aberrant cell cycling and cell death, likely leading to the microcephalic phenotype that is observed in the *ice1* mutant.

4.2. Gene expression analysis of neural stem cells in the *ice1* mutant

4.2.1. Whole head RNA-sequencing analysis of *ice1* mutants

I analyzed global RNA-seq data taken from 4dpf *ice1* mutants. cDNA libraries were generated from total RNA by Natalie Sorfazlian using whole heads from *ice1* mutants and siblings in 3 experimental replicates. Gene expression, intron retention, and 3' UTR retention were expressed as a $\log_2$ fold change coefficient in mutants compared with siblings with a wild-type phenotype. Genes were classified by GO term and marked as either upregulated or downregulated. Abundance of transcripts associated with cell cycle, transcription, and the nervous and visual system genes was overall decreased; conversely, transcripts of genes involved in splicing, apoptosis, signal transduction, and stress response was overall increased (Figure 4.8). Within splicing genes, the LEC components ICE1, SNAPC, and USPL1 were found to be increased in transcript abundance.

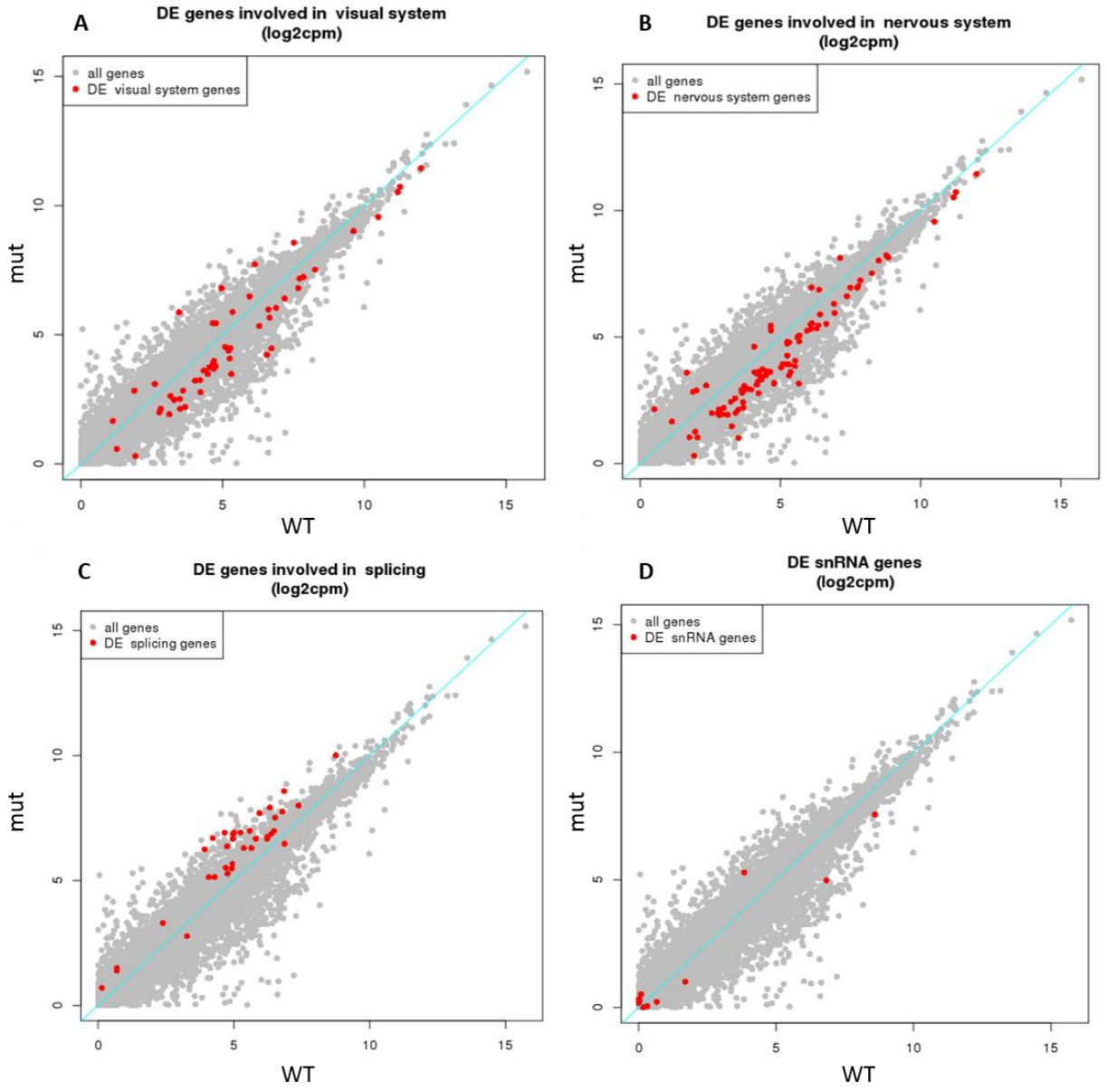

Figure 4.8 *Differentially expressed (DE) genes by subset in the* ice1 *mutant compared with wild-type.*

RNA sequencing results for DE genes associated with visual system, splicing, nervous system, and snRNA genes (in red) expressed as $\log_2$cpm. Genes involved in the visual system and nervous system are generally decreased (A,C), whereas splicing genes are overall increased (B). snRNA transcript levels could not be reliably analyzed in the *ice1* mutant (D). Analysis was performed in collaboration with Dr. Yunchen Gong.

Ice1 abundance was increased approximately 4-fold in mutants compared with siblings; this has been corroborated by *in situ* hybridization (Sorfazlian 2015). Transcript abundance of *Snapc4*, a protein which recognizes snRNA promoters (Takahashi et al. 2015), was increased nearly 6-fold in mutants. *Uspl1*, a transient LEC interactor (Hutten et al. 2014), was found to be 2.5 times more abundant in mutants. Transcript levels of the ICE1 binding partner ELL (*ell2*), on the other hand, was reduced by approximately 70% in the *ice1* mutant. Notably, p53 (*tp53*) transcript levels were increased over 8-fold in the mutants; this may be in part due to the reduction of ELL, which when highly expressed acts as a negative regulator of p53 transcription (Shinobu et al. 1999). It has also been shown that overexpression of p53 in cells lines leads to LEC repression by interfering with ELL-ICE1 binding (Anwar et al. 2016).

Of the 4865 genes included in the analysis, *ice1* mutants were found to express 181 genes (3.7%) with retained introns and 141 genes (2.9%) with retained 3' UTR compared with siblings. A list of over-represented GO terms with upregulated and downregulated genes containing retained introns (Appendix B) and retained 3' UTRs (Appendix C) have been included. At least within a small subset of genes, there is evidence of missplicing and intron retention in the *ice1* mutant.

While informative, there are some limitations to this approach. Though the RNA extraction method used for this experiment includes total RNA sequencing, transcripts from only a few snRNA genes were able to be detected using this method (Figure 4.8). Within the current study, the snRNAs detected in the RNA-seq would be far from representative of snRNA levels as a whole. In the future, using an RNA extraction method specific for small RNAs may improve snRNA capture and provide a more representative view of differential expression in the *ice1* mutant.

Another limitation is that these data were collected from whole head samples, which in essence contain a mixture of stem cells and differentiated cells primarily from brain and retina. Since it is unknown whether the *ice1* mutation has specific effects on neural stem cells, these results might actually reflect a mixture of changes in stem cells and differentiated cells. Stem and progenitor cell populations appear to be more profoundly affected by the loss of *ice1* compared to differentiated cells, but this still remains to be corroborated by other means.

Overall, the global RNA-seq analysis provides novel insight into the broad requirement of *ice1* in regulating gene expression. Transcript abundance of visual, nervous system, and cell cycle genes are decreased, consistent with the observed mutant phenotypes, while splicing genes are increased, likely as a compensatory mechanism. Evidence of missplicing in the mutant is demonstrated by intron and 3' UTR retention in a subset of mRNA genes.

4.2.2. Generation of an *ice1* radial glia specific fluorescent reporter line

The neural stems cells in the CMZ are progressively lost in the *ice1* mutant. By 4dpf, when mutants become morphologically distinguishable, there has already been significant loss of this stem cell population. In contrast, the radial glial cells in the forebrain and retina still appear to be present in the *ice1* mutant. This allowed the opportunity to expand on the role of *ice1* in a neural stem cell population. To this end, I generated an *ice1* heterozygous radial glia-specific line, *ice1*$^{+/-}$*;Tg(her4.1:mCherry)*. *Her4.1*, orthologous to mammalian *hes5*, is a downstream Notch signaling target and is highly expressed in radial glia of the central retina and forebrain PVZ. (MacDonald et al. 2015). I crossed the *Tg(her4.1:mCherry)* line with *ice1* heterozygotes and scored progeny for mCherry fluorescence after 2dpf. mCherry fluorescent larvae were raised to adulthood and genotyped by fin clip for *ice1* heterozygosity. In-crossing *ice1*$^{+/-}$*;Tg(her4.1:mCherry)* results in

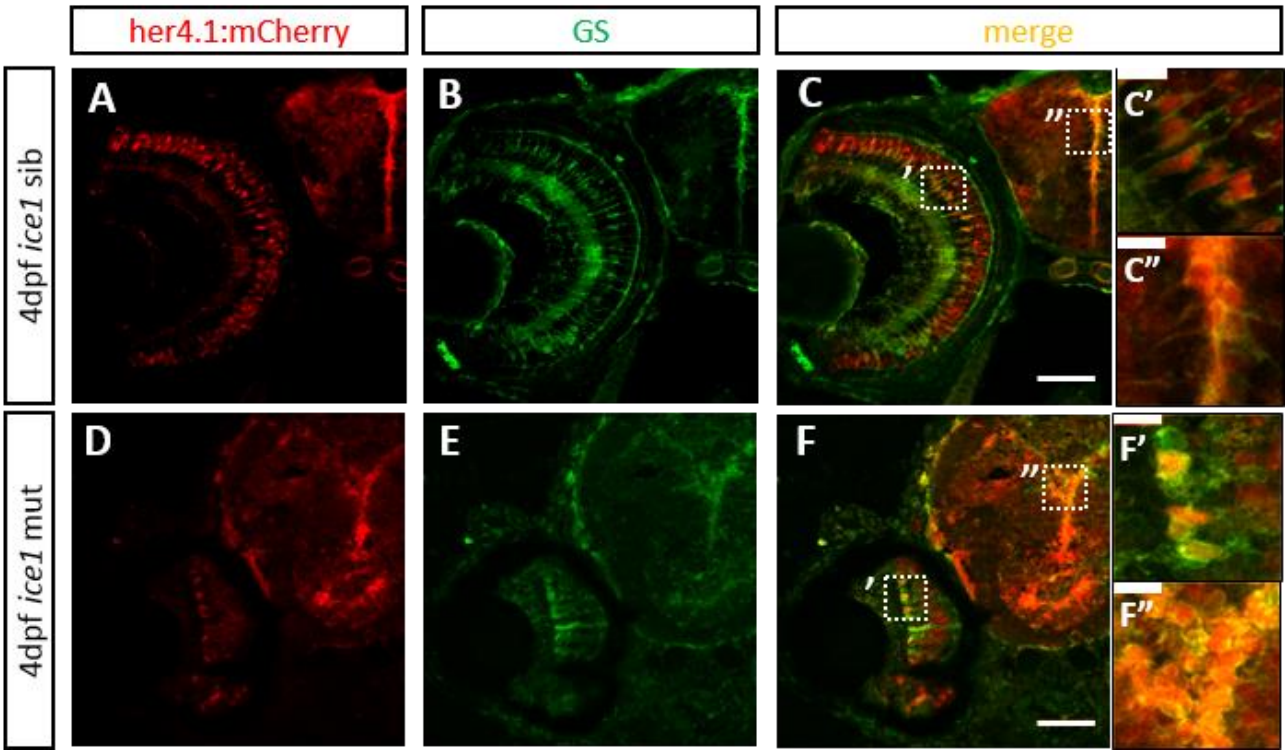

Figure 4.9 *Radial glia-specific fluorescence in* ice1 *sibling and mutant backgrounds.* *Her4.1*-driven mCherry fluorescence in the *Tg(her4.1:mCherryT2ACreERT2)* line demonstrates radial glia-specificity by co-staining with glutamine synthase (GS) in *ice1* siblings and mutants. Expression is shown in both Müller glia in the retina (C', F')) and radial glia in the PVZ (C", F"). Scale bar = 50µm (A-C, D-F); 10µm (C'-C", F'-F").

25% *ice1* mutant progeny which retain *her4.1*-driven mCherry fluorescence. Radial glia-specific fluorescence in the *ice1* mutants and siblings was confirmed by immunohistochemistry. The mCherry reporter fluorescence co-stains with glutamine synthetase, another radial glia marker, in the central retina and forebrain PVZ of both *ice1* siblings and mutants at 4dpf (Figure 4.9).

4.2.3. Validation of a radial glia isolation protocol using fluorescence activated cell sorting

To more specifically explore the influence of *ice1* within radial glia, I optimized a cell dissociation protocol, which was successfully used with fluorescent-activated cell sorting (FAC sorting) to enrich for radial glial cells to be used in downstream gene expression analysis. In addition to the *Tg(her4.1:mCherry)* line, I used a second radial glial cell-specific line, *Tg(GFAP:GFP)*, which showed somewhat higher background fluorescence and was therefore less desirable for the current study; however, this line was still quite useful for protocol validation (Figure 4.10, Figure 4.11).

4dpf larvae were screened by mutant phenotype and 30-40 heads were dissected from *ice1* mutant and sibling groups. A subset of tails were taken from each sample and individually sequenced to confirm genotypes. Head tissue was dissociated using papain enzyme and cells were treated with DAPI to mark non-viable cells. FAC sorting was conducted on live cells at the Faculty of Medicine Flow Cytometry Facility (University of Toronto). Four cell populations were collected: 1) mutant mCherry+ radial glia, 2) mutant mCherry- non-radial glia, 3) sibling mCherry+ radial glia, and 4) sibling mCherry- non-radial glia (Figure 4.12). Sorted cells were collected directly into TRIzol reagent for RNA extraction and cDNA synthesis. Samples were standardized by cell number before RNA extraction and then by amount of RNA added to the

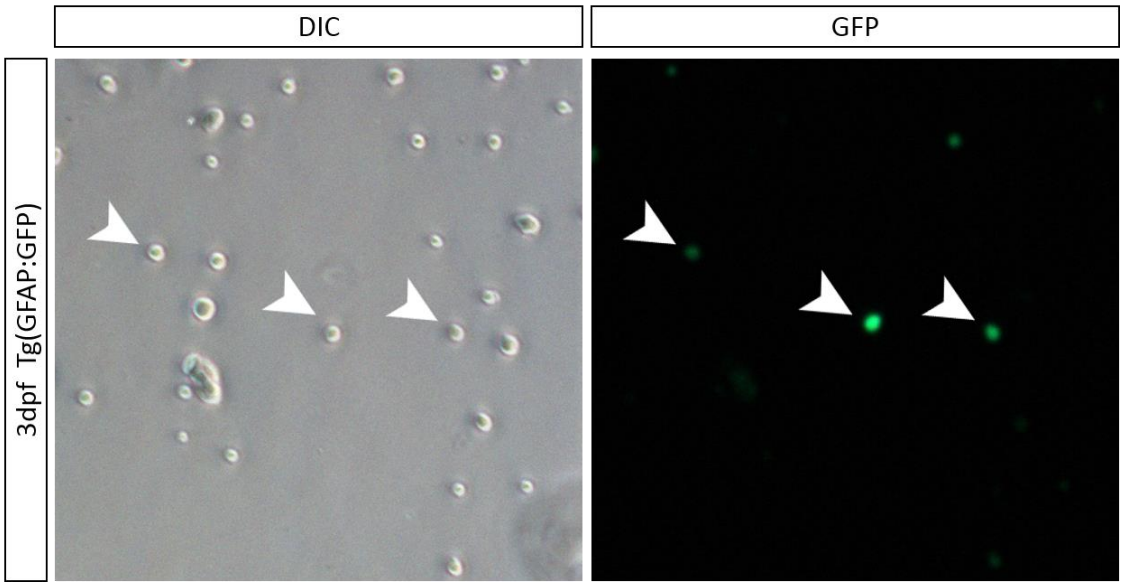

Figure 4.10 *Cell dissociation of larval zebrafish whole heads.*
Cell dissociation of whole heads using papain enzyme was tested using the Tg(GFAP:GFP) line, a fluorescent reporter of radial glia cells. Arrowheads denote individual GFAP:GFP+ cells.

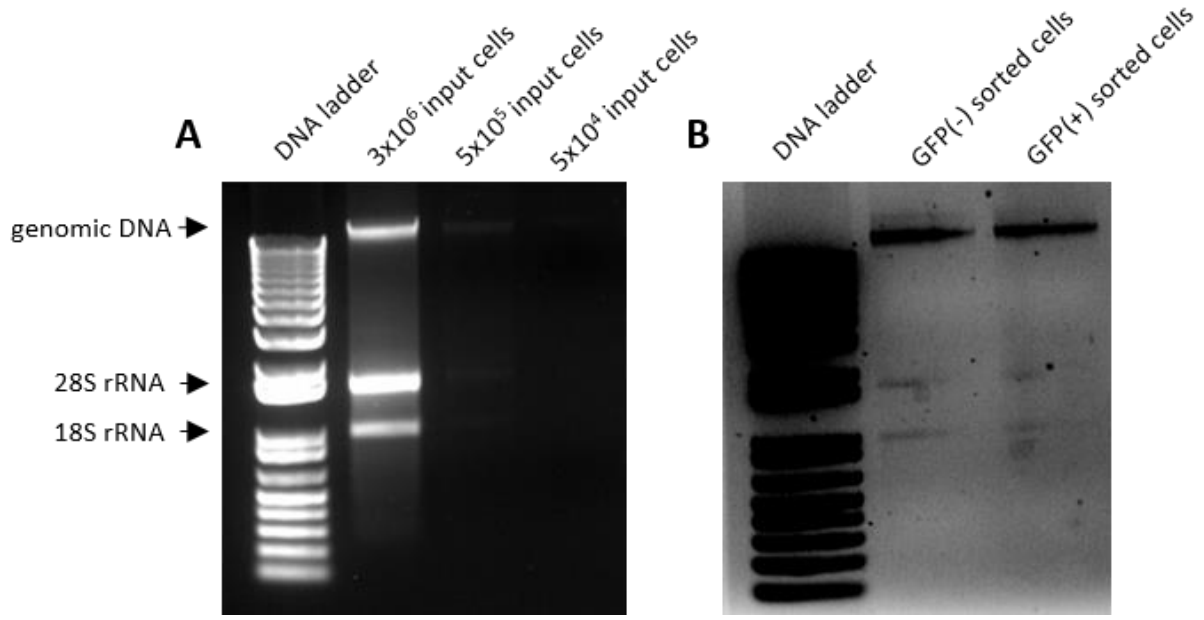

Figure 4.11 *Input cells and FAC sorted cells yield high quality RNA for downstream applications.*
RNA quality was tested in varying numbers of input cells (A) and in FAC sorted cells (B). Strong 28S and 18S rRNA bands were detected for $3x10^6$ input cells, but RNA levels were too low to be reliably detected for lower input levels. After FAC sorting, samples of $1x10^6$ GFP(-) and (+) cells both demonstrated consistent 28S and 18S rRNA bands.

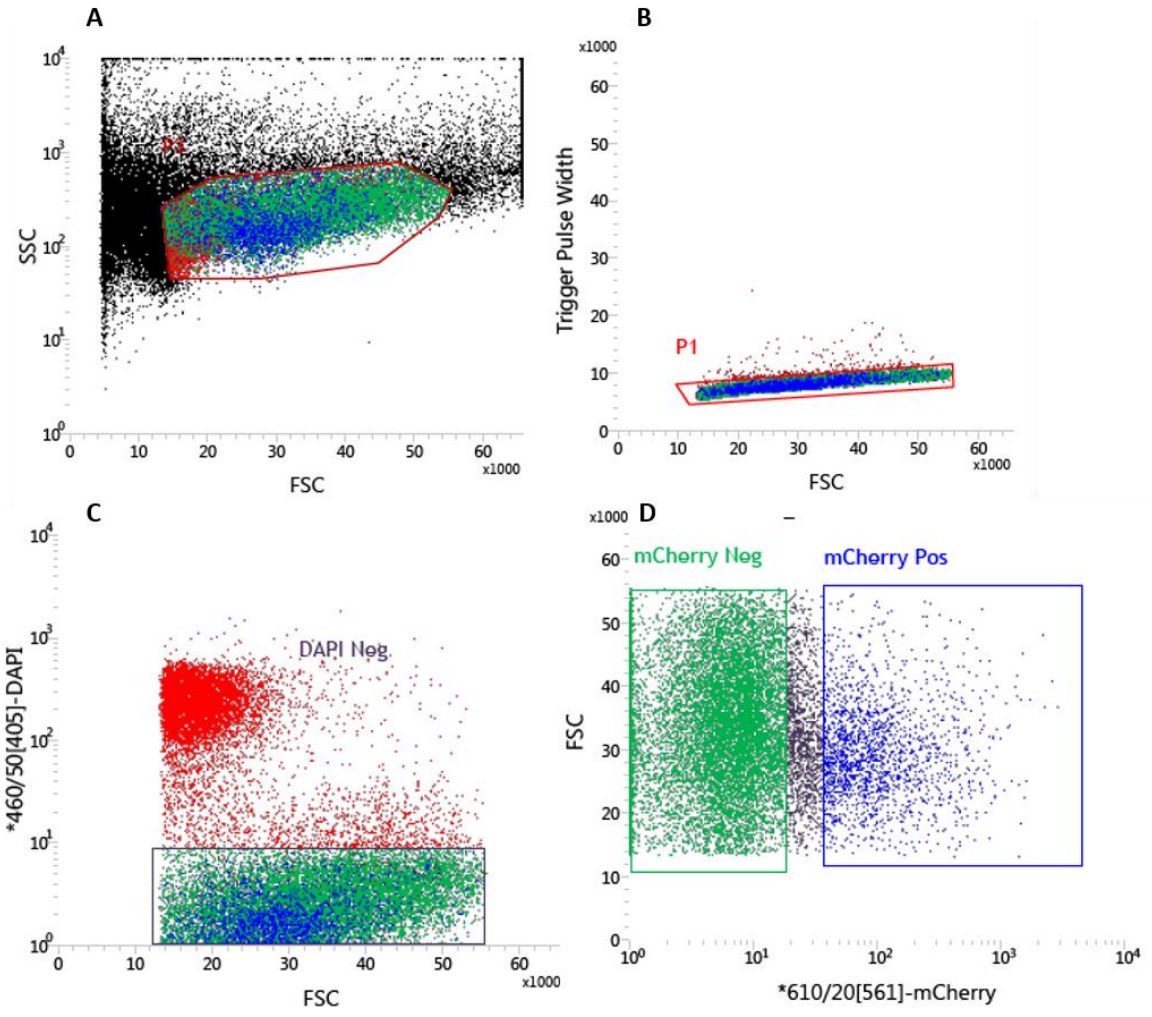

Figure 4.12 *Fluorescence activated cell (FAC) sorting of radial glia.*
Dissociated cells were selected for by size (A) and trigger pulse width (B) to ensure only single, unclumped cells were being sorted. Of these, only viable DAPI-negative cells (C) were selected for sorting into mCherry-positive and -negative groups (D). mCherry-negative gating was determined using a wild-type sample. FAC sorts were conducted using a 100µm nozzle at 17psi on a BD Influx at the University of Toronto.

reverse transcription reaction to ensure that relative proportions of gene transcripts between sample groups would be representative for direct comparison between groups.

4.2.4. Gene expression analysis of isolated radial glia in the *ice1* mutant

Real-time quantitative PCR was used to determine relative transcript abundance levels between cell populations for a select group of genes. I designed primers to test three classes of genes: 1) radial glia genes; 2) splicing-associated genes; and 3) snRNA genes. All expression levels are normalized to the RNA Pol I-transcribed 18S rRNA and three technical replicates were performed for three biological replicates of each cell population. Relative transcript abundance is compared within each biological replicate to account for differences between experimental runs. Significant differences between groups was determined by one way ANOVA and Tukey's post hoc multiple comparison analysis (Graphpad Prism).

To demonstrate that the FAC sorting was working consistently, I examined the levels of glutamine synthetase (*glula*), a radial glia-specific gene, in the sorted cell populations. As expected, *glula* was significantly enriched ($p < 0.0001$) in both sibling and mutant mCherry+ samples. There was no significant difference detected between the sibling and mutant mCherry+ populations. This indicates both that the FAC sorting is enriching for radial glia, and that the *ice1* deficiency does not appear to have an effect on radial glial identity at this (Figure 4.13).

4.2.5. The LEC interactor *uspl1* is increased in the *ice1* mutant

Previous studies in zebrafish have shown that splicing defects can induce a compensatory mechanism which upregulates a host of splicing-related genes (Trede et al. 2007). Our RNA-seq

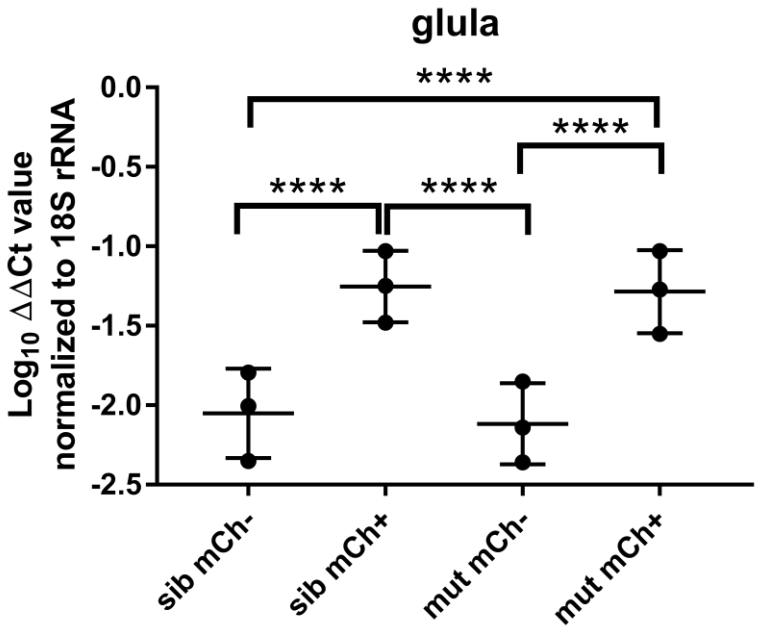

Figure 4.13 *The radial glia gene glula is significantly enriched in ice1 sibling and mutant sorted radial glia.*
Real-time qPCR was used to determine relative transcript levels normalized to 18S rRNA. Asterisks denote significance of p-value < 0.0001 (****) by ANOVA. Sib = *ice1* sibling; mut = *ice1* mutant; mCh- = mCherry- differentiated neurons; mCh+ = mCherry+ radial glia.

analysis revealed increased transcript abundance of numerous splicing-related genes in the *ice1* mutant (Figure 4.14). I wanted to investigate whether this increase in splicing genes would be more pronounced in radial glial stem cells in contrast to other cell types. I chose two splicing genes which are associated with the LEC pathway: *sart3*, also called *p110*, the U4/U6 snRNP recycling factor (Trede et al. 2007); and *uspl1*, a transient LEC interactor (Hutten et al. 2014). While *sart3* does not show any significant differential transcript abundance across groups, *uspl1* is significantly increased ($p < 0.05$) in both mutant cell populations (Figure 4.14). No significant difference was found between mutant radial glia and non-radial glia, which suggests a global increase of *uspl1* transcription in the mutant.

4.2.6. Higher snRNA levels are conserved or increased in mutant radial glia

In vitro, *ice1* has been shown to be an essential LEC component involved in RNA Pol II-transcribed snRNA genes. Here, I have tested the *in vivo* expression of U1, U2, U6, and U11 snRNA in radial glia and non-radial glia cells in both the *ice1* sibling and mutant background. U1 and U2 snRNAs are components of the major spliceosome and are highly repeated throughout the genome (Egloff et al. 2008). In contrast, U11 snRNA is a single copy gene in zebrafish which belongs to the minor spliceosome (Pessa et al. 2008). U6 is transcribed by RNA Pol III and purported to be LEC-independent, although RNA Pol II appears to play a regulatory role in proper U6 snRNA expression (Listerman et al. 2007; Smith et al. 2011).

Within the *ice1* siblings, I found significantly higher baseline levels of U1 snRNA in radial glia compared with non-radial glia cells (Figure 4.15A). There appears to be no significant difference in baseline levels of the other snRNAs between radial glia and non-radial glia cells. Within the *ice1* mutants, however, U1, U6, and U11 snRNA levels were significantly higher

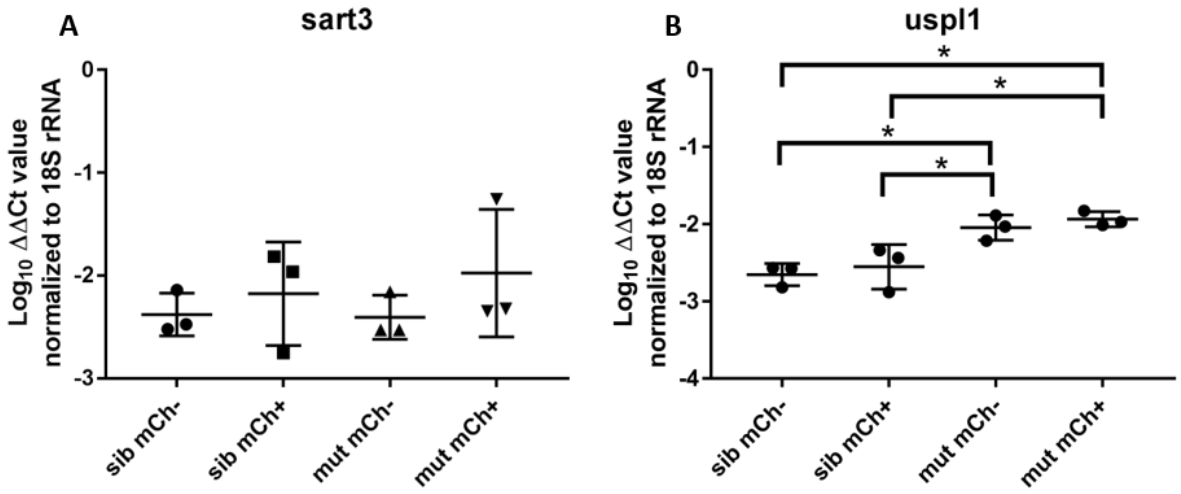

Figure 4.14 *The LEC interactor uspl1 is globally upregulated in ice1 mutants.*
Real-time qPCR was used to determine relative transcript levels normalized to 18S rRNA. Asterisks denote significance of p-value < 0.05 (*) by ANOVA. Sib = *ice1* sibling; mut = *ice1* mutant; mCh- = mCherry- differentiated neurons; mCh+ = mCherry+ radial glia.

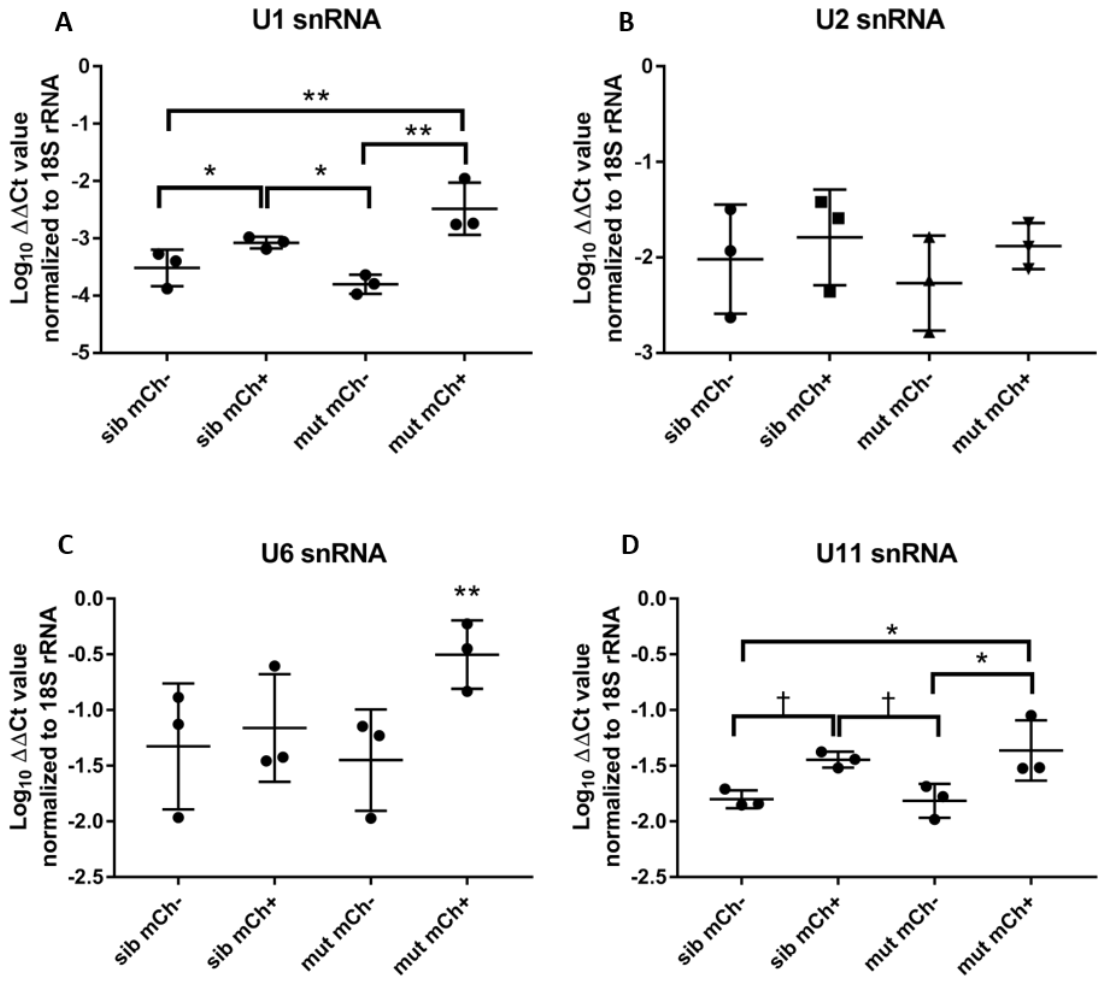

Figure 4.15 *The snRNA genes in ice1 sibling and mutant sorted cell populations.*
Real-time qPCR was used to determine relative transcript levels normalized to 18S rRNA. Asterisks denote significance of p-value < 0.05 (*) and 0.01 (**) by ANOVA. † denotes nonsignificant difference with p-value < 0.07. Sib = *ice1* sibling; mut = *ice1* mutant; mCh- = mCherry- differentiated neurons; mCh+ = mCherry+ radial glia.

($p < 0.01$) in the radial glia compared with non-radial glia cells (Figure 4.15). Across genotypes, only U6 snRNA levels were significantly increased ($p < 0.05$) in the mutant radial glia compared with sibling radial glia. Otherwise, there was no significant differential transcript abundance detected within radial glia in mutants compared with siblings. These data suggest that, at least within radial glia, *ice1* deficiency does not negatively affect transcript levels of Pol II-transcribed snRNA genes, but may in fact increase levels for some snRNA genes.

Our lab previously showed 60-70% reduction in U1 and U11 snRNA abundance in the 4dpf *ice1* mutant compared with wild-type (Sorfazlian 2015). I noted a consistent but non-significant trend of approximately 50% reduction in U1 and U2 snRNA abundance in the mutants (Figure 4.15A,B). It therefore seems likely that the previously observed decreased in snRNA levels in *ice1* mutants is limited to the non-radial glia cells, which would have masked the differential abundance now observed in the much smaller radial glia population.

4.3. Testing the early Müller glia dedifferentiation response in *ice1* mutants

In the normal retina, Müller glial cells are relatively quiescent and only sporadically dedifferentiate and divide to contribute to the rod photoreceptor lineage. However, in response to injury, Müller glia near the lesion will be recruited into a regenerative response causing them to dedifferentiate and divide to replenish lost neurons. This response requires rapid transient upregulation of genes associated with retinal stem cells including *pax6*, *vsx2*, and *rx1*, as well as partial downregulation of Müller glial identity genes (Raymond et al. 2006). Given that the *ice1* mutant CMZ cells show evidence of cell cycle arrest, I was interested in testing whether activated Müller glia would show a similar defect. To this end, I used a UV lesion paradigm (UV40) to induce photoreceptor death in *ice1* siblings and mutants at 4dpf, using EdU to detect cells that had dedifferentiated and re-entered the cell cycle. These were compared to control sibling and mutant

larvae from the same cohort but not exposed to UV light. Previous pilot studies in the lab have shown that injury-induced Müller glia dedifferentiation begins within 24 hours post lesion (hpl). I therefore allowed a 24hr recovery period and performed a 6hr EdU pulse to capture cells undergoing S-phase at 30hpl. EdU+/mCherry+ co-labeled cells in the central retina would be expected to mark actively proliferative Müller glia, whereas EdU+ cells adjacent to an mCherry+ cell would indicate an early progenitor cell presumably derived from the dedifferentiated Müller glial cell.

4.3.1. Control retinas are comparable to untreated retinas for both genotypes

Photoreceptors are normally arranged along the outer layer of the retina. Zpr1 staining, which marks red/green cone photoreceptors, is contiguous in both control *ice1* siblings and mutants (Figure 4.16). Control siblings exhibited very rare or absent detection of single EdU+ cells in the central retina (Figure 4.17A). Any EdU+ cells observed in the central retina either co-labeled with or were directly adjacent to mCherry+ Müller glia. Similarly, detection of EdU in the central retina was absent in control mutants (Figure 4.17B). Although the mutant retina is smaller, the proportion of mCherry+ Müller glia in the mutant was not significantly different from that of the sibling when corrected for size. However, the extensive variation in the number of mCherry+ cells (Figure 4.17E) in the mutant with our sample size suggests that there may indeed be a difference in the baseline number of Müller glial cells in the *ice1* mutant that could be revealed with increased sampling.

4.3.2. *Ice1* mutants fail to undergo early dedifferentiation response

Extended exposure to intense light induces widespread rod and cone photoreceptor death in the zebrafish retina (Vihtelic and Hyde 2000). My preliminary experiments show that Zpr1 staining was discontinuous in UV40 treated siblings and mutant (Figure 4.18), indicating that the

UV lesion was able to cause photoreceptor death. Müller glia in UV40 siblings appeared to dedifferentiate and re-enter the cell cycle as expected, whereas UV40 mutants show no evidence of Müller glia injury response (Figure 4.19). EdU+ cells are detectable in the sibling central retina, either colabeling with or adjacent to mCherry+ Müller glia. In contrast, EdU is completely absent from the mutant central retina, indicating a lack of cell cycle re-entry at this time point.

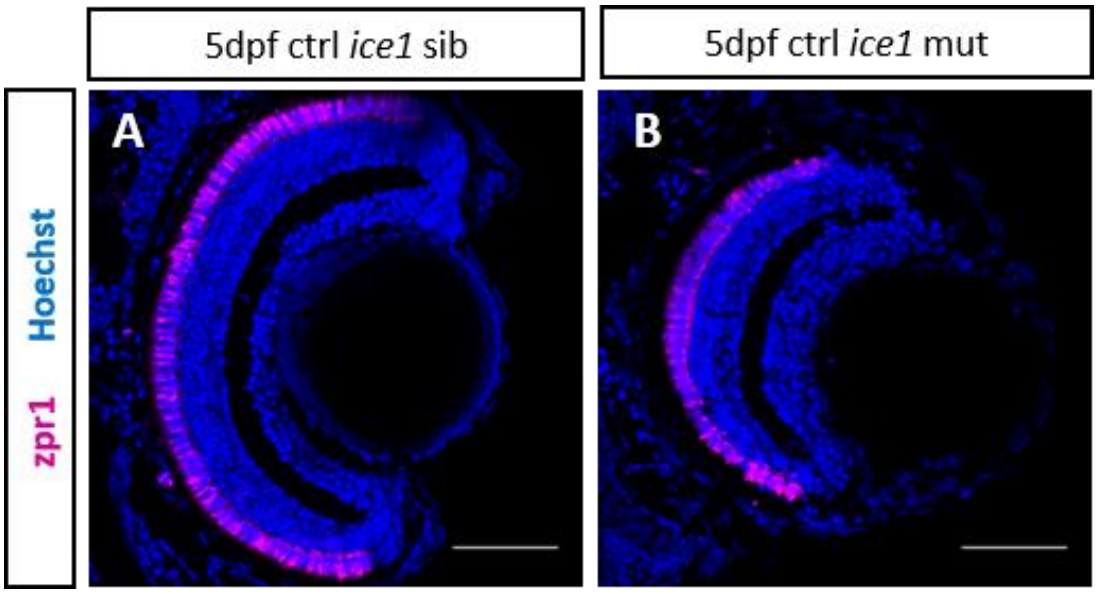

Figure 4.16 *Cone photoreceptor differentiation in untreated* ice1 *siblings and mutants.* Consistent staining for zpr1 (in magenta), a marker of cone photoreceptors, is observed along the outer layer of the retina in the *ice1* sibling (A). Comparable staining is also observed in the *ice1* mutant retina (B). Scale bar = 50µm.

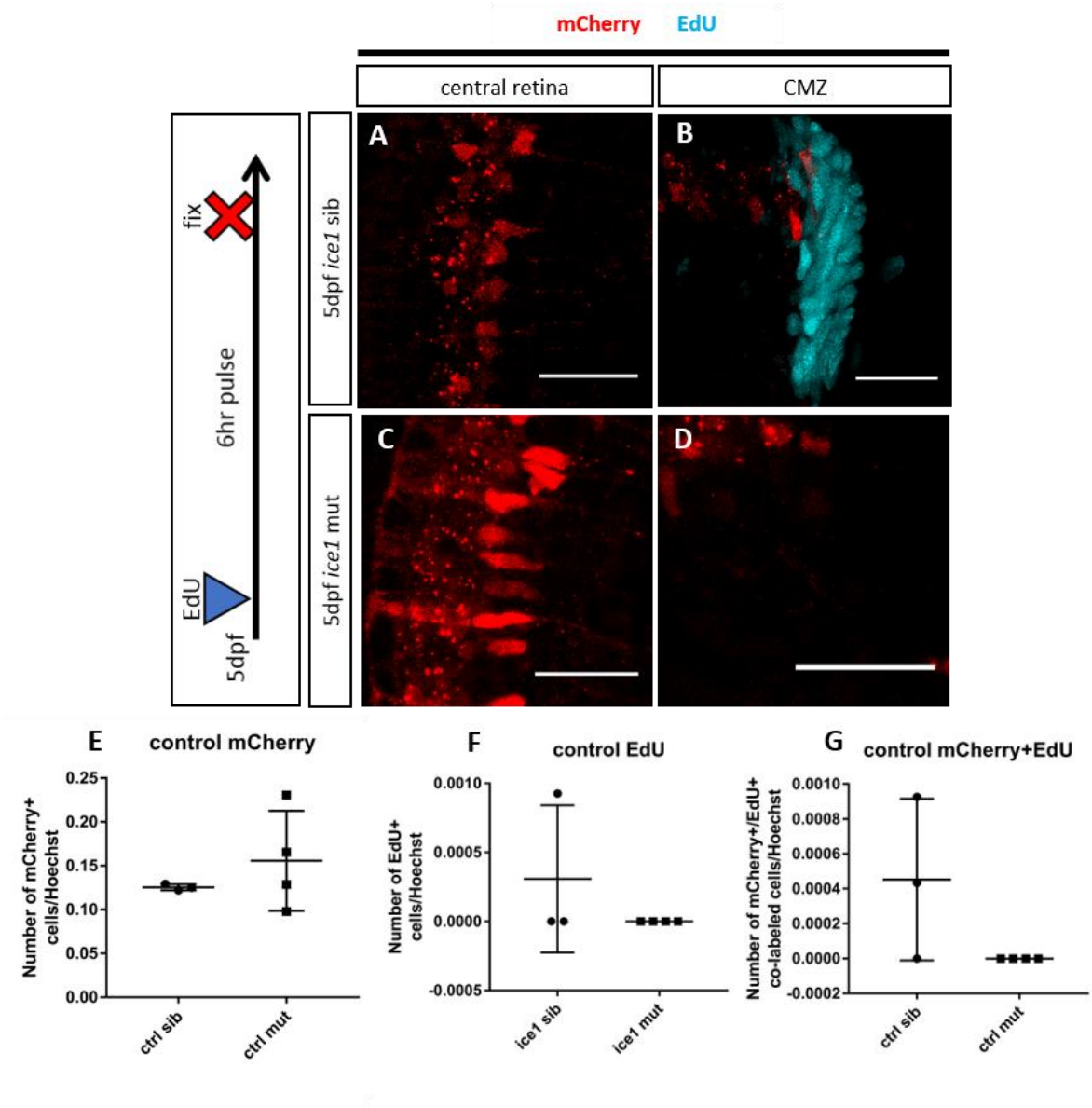

Figure 4.17 *Müller glia are not proliferative in the untreated* ice1 *sibling or mutant central retina.* EdU (in cyan) rarely co-labels with mCherry+ Müller glia (in red) in either the *ice1* sibling central retina at 5dpf (A), while EdU is detectable at the CMZ (B). In contrast, EdU+ cells are never detected in the *ice1* mutant central retina (C) or CMZ (D). Numbers of mCherry+ cells and EdU+ cells were quantified in the *ice1* sibling and mutant retinas (E-G). The proportions of mCherry+, EdU+, or mCherry+/EdU+ cells in the mutant central retina are not significantly different from the sibling. Scale bar = 20µm.

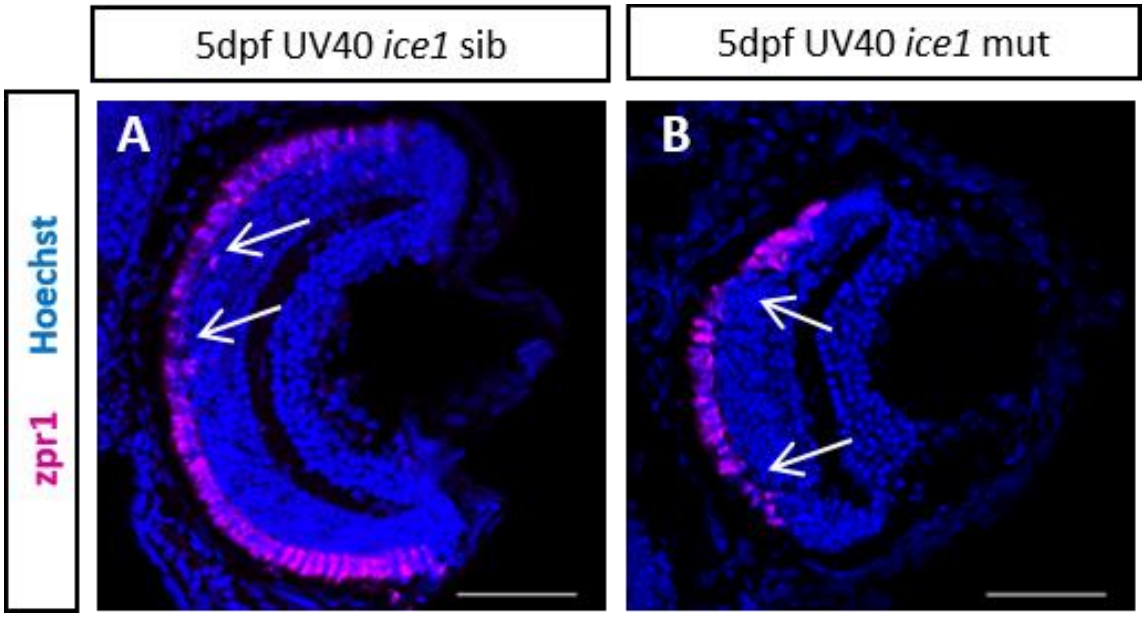

Figure 4.18 *Zpr1 staining is disrupted in UV lesioned* ice1 *siblings and mutants.*
Gaps in zpr1 staining (in magenta) observed along the outer layer of the retina in lesioned *ice1* siblings (A) and mutants (B) are likely due to cone photoreceptor death as a result of UV light treatment. Scale bar = 50µm.

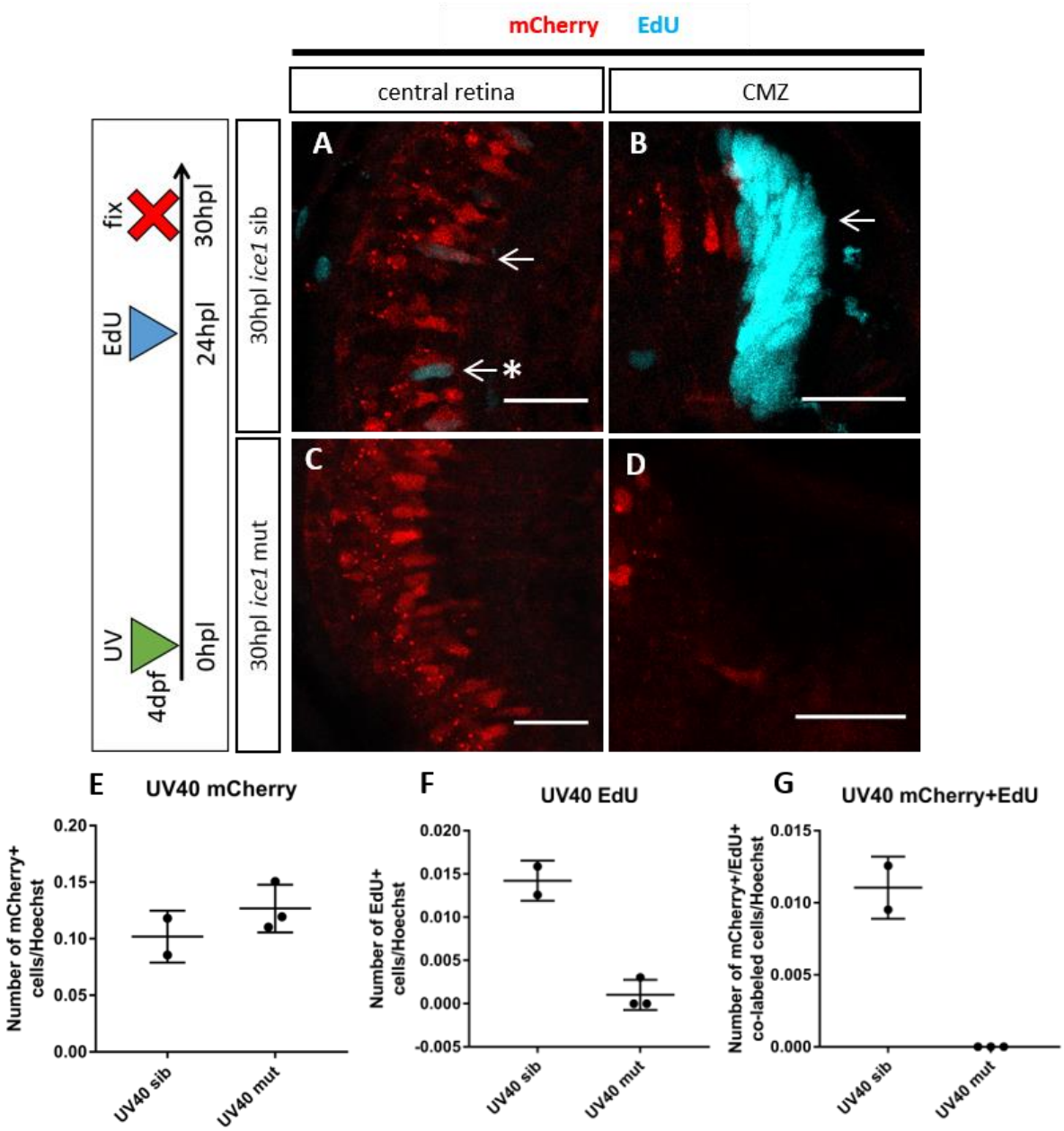

Figure 4.19 *Müller glia fail to undergo early dedifferentiation response to UV lesion in the* ice1 *mutant.*
EdU (in cyan) at 30hpl can be observed co-labeling with and adjacent to mCherry+ Müller glia (in red) in the *ice1* sibling central retina, indicative of the Müller glia cell cycle re-entry (A). As in untreated, no EdU can be detected in the *ice1* mutant central retina (C) or CMZ (D). Preliminary cell counts of mCherry+ (E) and EdU+ (F) cells appear to show higher EdU+ cells in UV40 siblings compared with mutants. Arrows denote mCherry+/EdU+ co-labeled cells; Arrows with asterisks denote mCherry+ adjacent EdU+ cells. Scale bar = 20µm.

Chapter 5
Discussion

5.1. Summary of Observations

The present work characterizes the first *in vivo* loss-of-function model of an essential LEC component, *ice1*, and its role in the maintenance of neural stem cells in the postembryonic zebrafish. My prediction was that neural stem cells have a greater need for splicing efficiency and are therefore more sensitive to *ice1* deficiency. Immunohistochemical analysis of the constitutively active CMZ and the relatively quiescent PVZ in the ice1 mutant shows that both stem cell compartments appear proliferative, but otherwise show significant reduction or absence of cell cycle markers coupled with an increase in apoptosis. This points to a cell cycle defect of the neural stem cells and their subsequent removal by apoptosis, which leads to the progressive loss of both stem cell pools. In contrast, the quiescent Müller glial cells of the mutant central retina appear comparable to the uninjured wild-type retina.

Transcriptomic analysis of the *ice1* mutant at the whole tissue level revealed a general increase in transcript levels of splicing related genes, including several LEC components, reminiscent of microarray analysis performed for the *earl grey* zebrafish mutant (Trede et al. 2007). This increase could be indicative of a compensatory mechanism to overcome *ice1* deficiency and maintain the level of splicing efficiency. In contrast, visual system, nervous system, and cell cycle genes were generally decreased. These findings fit with our model of mutant neural stem cells arrested in the cell cycle and removed by apoptosis, leading to progressive loss of the neural stem cell compartments and reduced growth of retina and forebrain tissues.

Since stem cells have unique requirements for maintenance, I isolated radial glia for gene expression profiling by RT-qPCR to specifically examine the effect of *ice1* deficiency on a neural

stem cell population. Transcript levels of the radial glial gene *glula* was found to be equally enriched in mCherry+ radial glia compared with mCherry- non-radial glia cells in both the *ice1* siblings and mutants. Similar to the RNA-seq findings, the LEC interactor *uspl1* was increased in both cell populations in the *ice1* mutant. Interestingly, however, the qPCR data point to cell-population specific effects for snRNA genes. U6 and U11 snRNA levels were higher in mutant radial glia in comparison to sibling and mutant non-radial glia. U1 snRNA levels were significantly higher in radial glia of siblings and mutants, whereas a nonsignificant trend points toward reduced levels of U1 and U2 snRNA in mutant non-radial glia cells. These data suggest that *ice1* may not have a role in regulating snRNA transcription *in vivo*, or that *ice1* may have LEC-independent roles.

The PVZ niche includes a large pool of relatively quiescent radial glial cells, which divide asynchronously. In contrast, the retinal Müller glial cells are largely silent except for contribution to the rod photoreceptor lineage at a low frequency. Normally quiescent Müller glia can be recruited into reactive neurogenesis by retinal lesion to replace damaged neurons. To further determine the role of *ice1* in activated versus quiescent stem cells, I tested whether injury-induced Müller glia activation in the *ice1* mutant would be inhibited. I demonstrated that while UV lesion was sufficient to induce widespread activation of Müller glia in *ice1* siblings, no activation of Müller glia was detected in *ice1* mutants. The apparent lack of dedifferentiation response in mutant Müller glia suggests that *ice1* is necessary for the maintenance of actively proliferating cell populations and highlights the link between *ice1* and cell cycle regulation.

5.2. *Ice1* deficiency leads to cell cycle arrest of actively proliferating neural stem cells

Previous studies in zebrafish have shown that by selectively interfering with snRNP function or its major proteins, cell proliferation is significantly reduced (König et al. 2007; Trede et al. 2007; Markmiller et al. 2014). The most severe phenotypes are observed in highly proliferative tissues including those in the eye, brain, and gut. Consistent with these studies, the *ice1* mutant exhibits cell cycling defects in proliferating cells in the retina and forebrain. To date, other organ systems in this mutant have not been studied and so future work will be required to determine if the cell cycle defects are present in all tissues.

As described above, PCNA is observed in both the mutant CMZ and PVZ neural stem cell compartments, which suggests that the cells remain in a "proliferative" state. The lack of EdU uptake and reduced number of PHH3+ cells, however, suggests that entry into S-phase and M-phase, respectively, is inhibited. The data suggest that mutant precursor cells in the brain as well as the retina are likely arrested in the G1 phase after their final round of mitosis. Nonetheless, it is also possible that mutant cells are arrested in the G2 phase of the cell cycle. As a result, these stem cells are unable to self-renew or contribute to the growth of the retina and forebrain, and are therefore removed by apoptosis. A G1-phase arrest would correlate with the decrease in the G1/S-phase transition marker *ccnd1* observed by *in situ* in the retina and forebrain as early as 3dpf. RNA-seq analysis showed downregulation of G1/S-phase cell cycle transition genes in the *ice1* mutant, including *ccnd1, ccne1*, and *ccne2*, and strong upregulation of p53.

The p53 pathway has been previously linked to cell cycle arrest in the context of disrupted splicing. An *in vitro* study demonstrated that interfering with the spliceosome by siRNA knockdown of key proteins results in increased p53 protein levels and p53 transcription

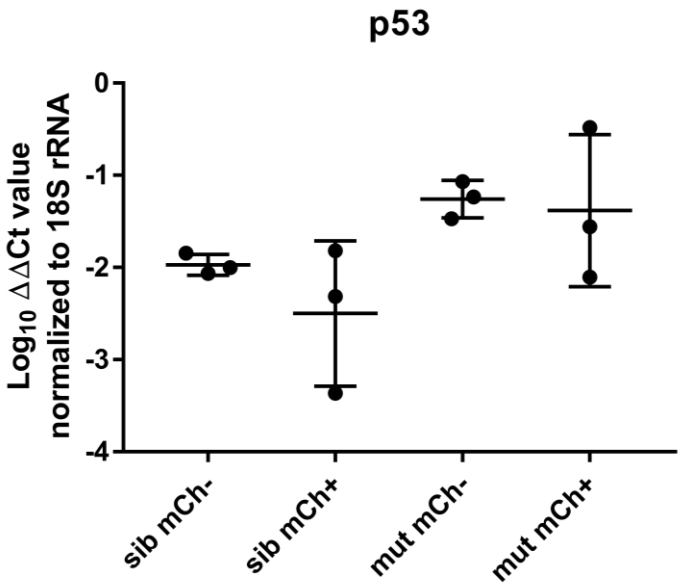

Figure 5.1 *p53 gene expression levels appear upregulated in the* ice1 *mutant.*
Real-time qPCR was used to determine relative transcript abundance normalized to 18S rRNA. Though no significant differences ($p < 0.05$) were detectable by ANOVA, there is a trend toward increased levels observed in both *ice1* mutant cell populations. Sib = *ice1* sibling; mut = *ice1* mutant; mCh- = mCherry- differentiated neurons; mCh+ = mCherry+ radial glia.

and led to an accumulation of G1-phase arrested cells (Allende-Vega et al. 2013). In postnatal mice, selective deletion of the splicing regulator PRMT5 in neural stem and progenitor cells resulted in defective pre-mRNA splicing of genes involved in cell cycle progression (Bezzi et al. 2013). Neural progenitor cells exhibited loss of self-renewal and increased apoptosis in the dorsal forebrain; but PRMT5 deletion in a p53 null background was able to partially rescue this phenotype (Bezzi et al. 2013).

p53 levels were found to be increased in the *ice1* mutant approaching statistical significance in mCherry+ radial glial and mCherry- non-radial glial cell populations (Figure 5.1). Similar to the *uspl1* data, the p53 increase in the mutant appears to be global as opposed to a cell-specific effect. A global increase in p53 levels is likely in part responsible for the cell cycle defects observed in the mutant neural stem cell populations and triggering widespread apoptosis in both proliferative and non-proliferative cells. However, these experiments would need to be repeated to confirm that the increased levels in the mutant is statistically significant and consistent with the RNA-seq data. Whether the higher level of p53 is interfering with splicing by disrupting ELL, either in its role with the LEC or SEC, requires further investigation.

5.3. Radial glia appear genetically resilient to *ice1* deficiency

Studies in human and *Drosophila* immortalized cell lines have demonstrated that ICE1 is an integral scaffolding component of the LEC which is required for snRNA gene transcription (Smith et al. 2011; Hu et al. 2013; Takahashi et al. 2015; Anwar et al. 2016). Previous work from our lab showing decreased levels of U1 and U11 snRNA transcript levels in the *ice1* mutant suggested that the function of *ice1 in vivo* might be conserved in zebrafish.

To date, *ice1* has only been associated with snRNA gene transcription via the LEC; however, my RNA-seq analysis of the *ice1* mutant demonstrates that RNA Pol II-dependent expression of mRNAs is affected as well. Cell cycle, visual system, and nervous system genes are all generally decreased in the *ice1* mutant. One potential explanation for these decreases is due to cell death of certain subpopulations of cells, affecting transcript abundance by reducing the number of cells. The phenotypic analysis of the mutant retina and brain show increased caspase-3 staining; however, subpopulations that are predominantly affected in the mutant (ie. CMZ stem cells, PVZ radial glia) are still present as demonstrated by PCNA staining. Thus, increased apoptosis cannot fully account for these decreases in transcript levels. Another explanation is that this may be a secondary effect of reduced snRNA production, whereby limiting essential spliceosome components leads to lowered overall splicing efficiency, including evidence of intron retention and missplicing. Increased levels of p53 could be interfering with ELL participation not only in the LEC, but in the SEC as well. It is worth noting that the U4/U6 snRNP recycling factor zebrafish mutant, *earl grey,* also found highly upregulated p53 levels by microarray analysis at 3 and 5dpf (Trede et al. 2007). The deleterious effects of *ice1* may therefore be twofold: first, in terms of reduced snRNA levels, which interferes with spliceosomal function; and second, by triggering the p53 pathway potentially causing SEC-dependent splicing defects through ELL inhibition as well as inducing apoptosis.

RT-qPCR analysis of FAC sorted radial glia and non-radial glia showed expected mutant differential expression in selected mRNA genes, based on the global RNA-seq results. The LEC interactor *uspl1* was upregulated in both mutant cell population compared with the corresponding sibling cell population.

FAC sorted radial glia appear to have a higher baseline level of U1 snRNA expression, which may reflect a greater burden for efficient splicing. Previous studies have provided evidence that stem cells have unique splicing requirements which contribute to their multipotency and self-renewal (Li et al. 2007; Yap et al. 2012; Hirsch et al. 2015). This may also be extended to differential expression of snRNA variants, which has been implicated in regulating stem cell maintenance and development. Individual snRNA variants have been shown to have distinct temporal and spatial expression over the course of development in a number of species (Lu and Matera 2014). U1 snRNA variants in particular have been implicated in maintaining stem cell pluripotency (Vazquez-Arango et al. 2016) as well as early development cell fate decisions (Cheng et al. 1997).

Most surprising was the finding that transcript levels of LEC-dependent snRNAs U1, U2, and U11 did not appear to be affected in the *ice1* mutant radial glia-enriched population. The mutant non-radial glia, however, demonstrated a consistent trend toward reduced U1 and U2 snRNA levels by approximately 50% (Figure 4.15A, B). This begs the questions: how are snRNA transcript levels maintained in radial glia cells, which show the most severe phenotype and in which LEC repression would be predicted to have the greatest effect? Why would the non-radial glia population, which predominantly consists of postmitotic differentiated neurons, exhibit evidence of reduced snRNA transcription? And what mechanistic explanations can reconcile these results?

One explanation could be that *ice1* is not essential for snRNA transcription *in vivo*, contrary to evidence from cell line assays. A molecular analysis of *ice1* function has yet to be conducted *in vivo* so this possibility cannot be ruled out. However, it seems unlikely that *ice1* function is not conserved since at the whole head tissue level, U1 and U11 snRNA levels were found to be

significantly reduced in the mutant. The similar pattern observed in U1 and U2 snRNA reduction in the mutant non-radial glia cells in my experiments (although not statistically significant), which would make up the majority of the tissue, suggests that snRNA transcription is being affected in the mutant, but that some cell types may be more sensitive to the loss of *ice1* function.

Another explanation is that the ice1 protein in our mutant zebrafish retains partial functionality (e.g. hypomorphic allele). Since radial glia appear to normally produce higher levels of snRNAs than non-radial glia, a partially functional ice1 protein may be sufficient to maintain transcription rates. This might be less evident in non-radial glial cells because their baseline requirement for snRNA transcription is lower and this could account for the further decline observed in U1 and U2 snRNAs. It is also unclear whether there is haploinsufficiency of our mutant allele. In most of our experiments we choose 'sibling' controls that are a mixture of wild type and heterozygous larvae since previous analyses indicated that heterozygous larvae had no overt signs of any defects. However, transcript levels may be partially altered (and qPCR is very sensitive to detect these changes) and this may have contributed to the variability detected in my RT-qPCR analyses. Future studies should separate all larvae by genotype.

Another possibility is that the *ice1* mutant is still able to transcribe snRNA genes, but those transcripts are defective at the 3' end. Normally, snRNA genes are not polyadenylated; instead, they contain a 3' recognition sequence (3' box) downstream of the coding sequence which is necessary for cleavage of the nascent transcript and subsequent nuclear export (Matera and Wang 2014). Proper 3' end maturation is dependent on the Integrator complex for cleavage of the transcript (Chen and Wagner 2010). 3' end processing is also dependent on the recognition of a snRNA promoter by RNA Pol II; promoter swapping experiments have revealed that use of a non-snRNA promoter causes misprocessing of the 3' end, which can include aberrant polyadenylation

(Neuman de Vegvar et al. 1986; Chen and Wagner 2010). Since we currently do not know whether *ice1* has defects in RNA Pol II recruitment at snRNA genes, it is possible that 3' box recognition may be affected, leading to abnormal polyadenylation of snRNA transcripts.

Although the function of *ice1* appears to be at least partially conserved in zebrafish, this has yet to be corroborated by protein analysis. Since no antibody for zebrafish ICE1 protein currently exists, a recombinant protein approach such as FLAG- or myc-tagged ICE1 would be necessary. This would be useful for visualizing ICE1 *in vivo* and confirming that the *ice1* mutant generates a truncated protein. To explore whether RNA Pol II recruitment is affected at snRNA genes, I performed a preliminary chromatin immunoprecipitation (ChIP) analysis on whole *ice1* sibling and mutant heads. RT-qPCR was then performed to determine relative amounts of RNA Pol II recruitment at snRNA genes. Actin was used as a control to demonstrate no differences between siblings and mutants (Figure 5.2A). Surprisingly, RNA Pol II recruitment at U1, U2, and U6 snRNA genes showed no significant differences between siblings and mutants (Figure 5.2B-D). These results are in direct opposition with previous *in vitro* ChIP analyses performed in ICE1 knockdown backgrounds, which suggest that ICE1 is essential for RNA Pol II recruitment at snRNA genes (Hu et al. 2013). However, my RT-qPCR data suggest that snRNA transcription is relatively unaffected in the *ice1* mutant, which is supported by no apparent change observed in RNA Pol II localization. Since the RT-qPCR data suggest that there may be cell type-specific effects, ChIP analysis on FAC sorted cell populations would be most informative. I would predict that cell populations where reduced gene expression was observed would correspond with lower levels of RNA Pol II at those gene promoters.

Previous RT-qPCR data at the whole head level showed a drastic reduction in U1 and U11 snRNA levels in the *ice1* mutant. Importantly, there are several technical differences which could account

for the discrepancy in the current data. Firstly, the method in tissue collection may be a factor in the observed snRNA expression differences between genotypes. Theoretically, the sorted mCherry- population is simply all non-radial glia taken from the head tissue; however, certain cell types might be preferentially collected over others, for instance based on size and resilience to the dissociation and sorting process. Furthermore, cell sorting based *her4.1* expression does not perfectly capture all radial glia. While the majority of *her4.1*-expressing cells are quiescent radial glia, *her4.1* expression is absent in small subsets of radial glia. For instance, radial glia in the midbrain lining the optic tectum do not appear to express *her4.1*, but express *her9* genes instead (Chapouton et al. 2011). In addition, *her4.1* has been detected to a lesser extent in some neuroblasts in the hypothalamus and midbrain (Chapouton et al. 2011). Thus, the mCherry- (*her4.1*-absent) cell population may include subsets of radial glia, and conversely the mCherry+ (*her4.1*-expressing) cell population may include some non-radial glial cells. This overlap could account for some of the variation observed in my RT-qPCR data and at the very least suggest that my mCherry- cell populations are not quite comparable to whole head tissue.

RT-qPCR transcript levels were normalized to different control genes which could have skewed the observed relative abundance levels. The whole head data was normalized to tubulin, whereas I normalized my FAC sorted cell data to 18S rRNA. The *ice1* mutant exhibits defects in epithelial integrity such as drastic reduction of β-catenin at photoreceptor cell junctions, suggesting disruption of adherens junctions (Figure 5.3).The apical tight junction marker ZO-1 and adherens junction marker crb2a were both previously demonstrated to be reduced in the *ice1* mutant as well (Sorfazlian 2015). Furthermore, the RNA-seq data revealed a downregulation of microtubule-associated cytoskeletal genes including tubulin itself (Appendix A). The large variation in expression of RpL13a, originally included to act as a LEC-independent small RNA control,

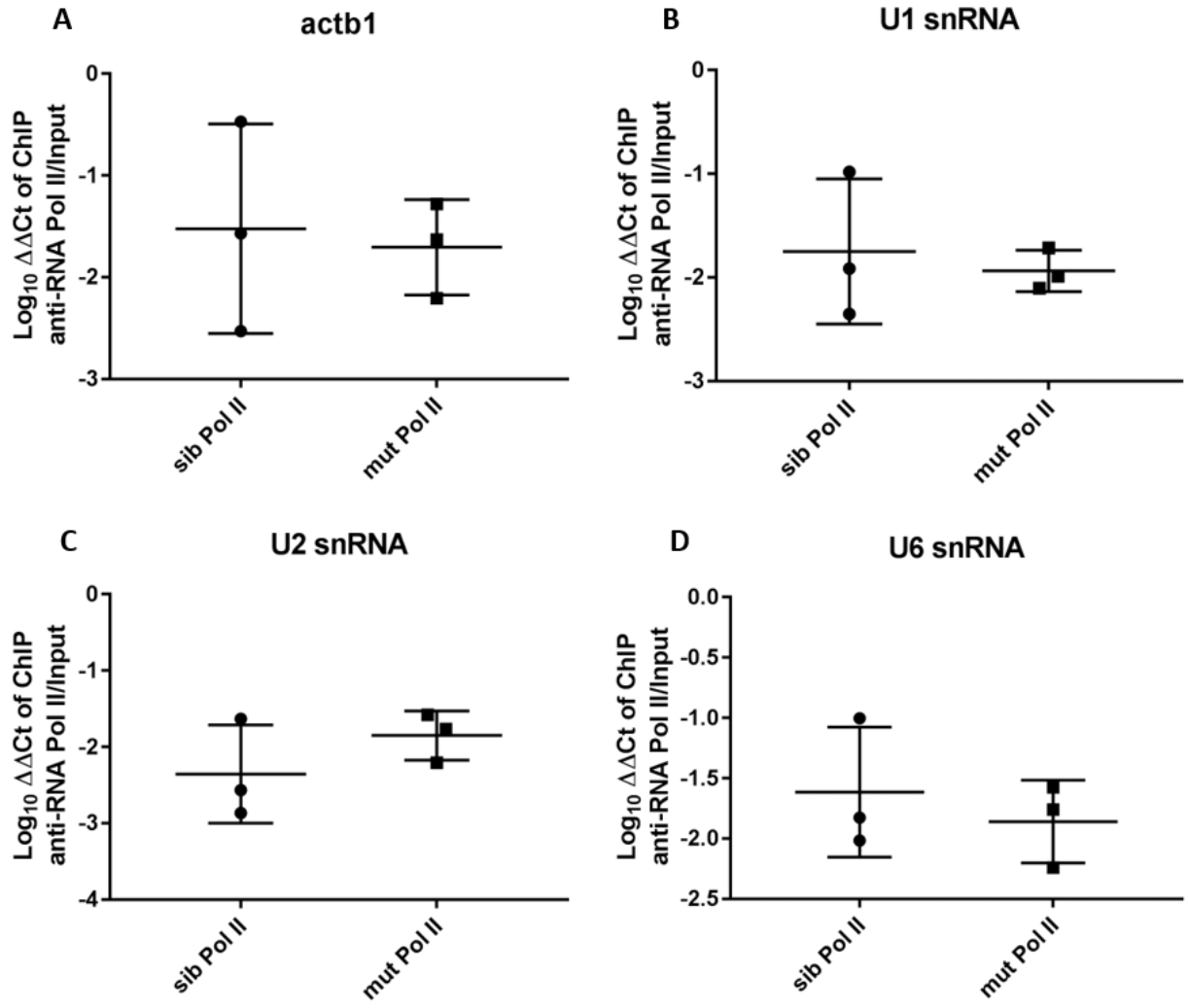

Figure 5.2 *RNA Pol II localization at snRNA genes does not appear to be affected in* ice1 *mutant whole heads.*
RT-qPCR demonstrating RNA Pol II occupancy at actin and the snRNA genes U1, U2, and U6 normalized to sample input. There was no significant difference observed in *ice1* mutants compared with siblings for any of the genes tested. Sib Pol II = *ice1* sibling, anti-RNA Pol II; mut Pol II = *ice1* mutant, anti-RNA Pol II.

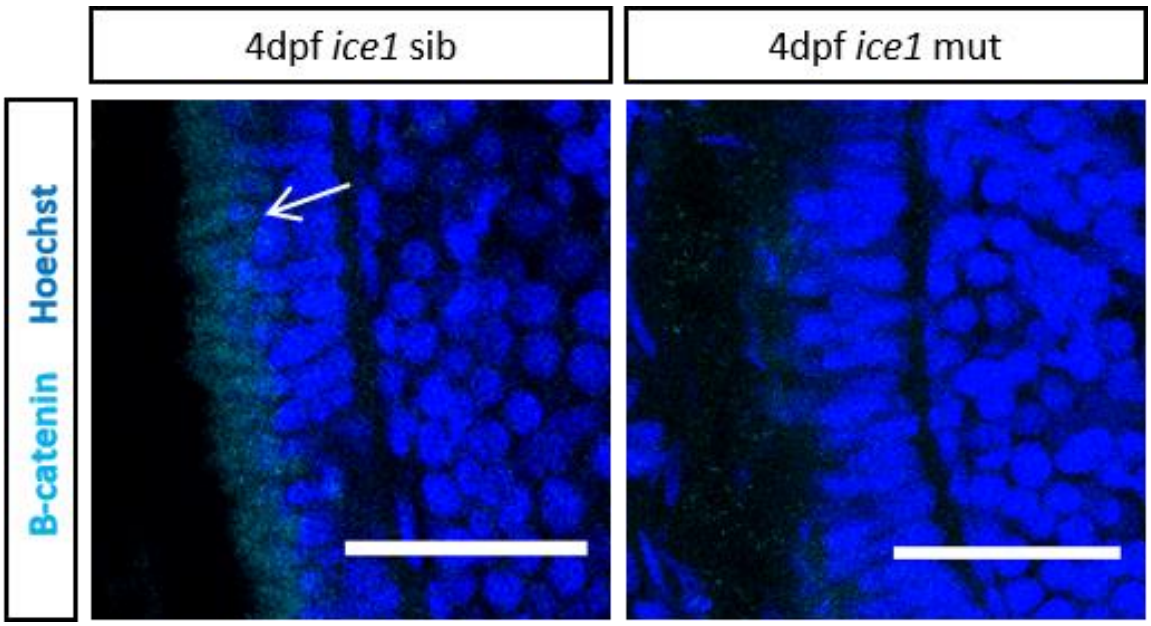

Figure 5.3 *β-catenin is drastically reduced at photoreceptor cell junctions in the* ice1 *mutant.* The adherens junction marker β-catenin (in cyan) is consistently detected along the apical side of the photoreceptor cell layer in the *ice1* sibling retina. β-catenin is virtually undetectable in the *ice1* mutant, suggesting possible defects in epithelial integrity. Scale bar = 20µm.

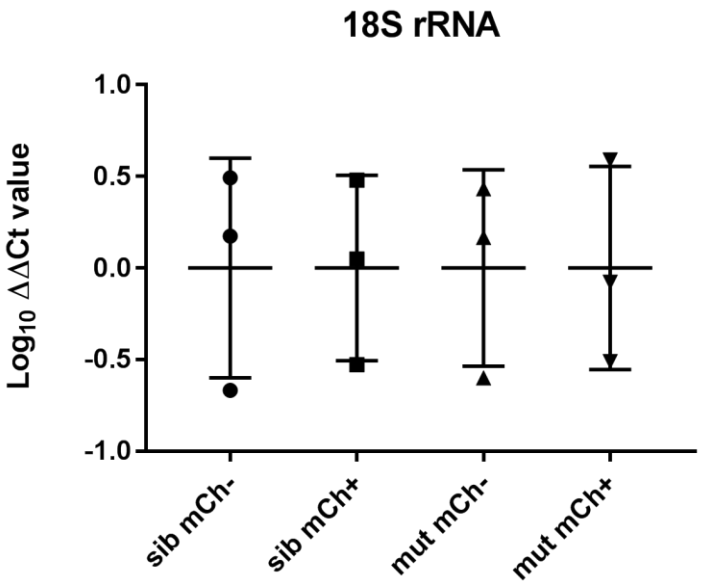

Figure 5.4 *Stable 18S rRNA expression in FAC sorted cell samples across biological replicates.* Real-time qPCR expression levels of 18S rRNA was comparable across biological replicates. No significant differences were detected between groups. Sib = *ice1* sibling; mut = *ice1* mutant; mCh- = mCherry- differentiated neurons; mCh+ = mCherry+ radial glia.

potentially points to the unsuitability of tubulin as a normalizing gene for this experiment (Sorfazlian 2015). In contrast, 18S rRNA is transcribed by RNA Pol I and is presumably not affected by LEC-dependent or -independent RNA Pol II activity. Relative abundance was consistent within biological replicates and no significant difference was found between cell populations or genotypes (Figure 5.4). In addition to using a different control gene, I designed new snRNA primer sets which may have affected the level of detection. The major spliceosomal snRNAs (U1, U2, U6) are highly repeated with slight sequence variations throughout the genome. Though many of the repeats are classified as pseudogenes, a number of these variants are actively transcribed. It is likely that different primer sets would pick up different snRNA variants, which may not have consistent expression levels.

The RT-qPCR and RNA-seq data point to a potential compensatory mechanism by increased transcription of splicing genes in the *ice1* mutant. It is possible that this compensation may in fact be enough to rescue defects in ice1's role in snRNA transcription, which could explain why no change was observed in LEC-dependent snRNA levels. Currently, though, it is unknown whether *ice1* has any LEC-independent functions that have yet to be characterized *in vivo*. Investigating other protein interactors of ice1, for instance through affinity purification mass spectrometry, would provide insight into any LEC-independent functions which may be linked to the mutant phenotype as well as confirm ice1's role in the LEC in our model.

The current FAC sorting protocol works successfully, but can be further improved for greater accuracy. I observed a consistent but nonsignificant trend toward downregulation in U1 and U2 snRNA expression in mutant non-radial glia cells. Adding more biological replicates would help to further resolve differential expression patterns and increase statistical power. The FAC sorted radial glia I obtained are a heterogeneous mixture of Müller glia and PVZ radial glia.

It is possible that some of the observed variability in transcript abundance is actually a reflection of the mixed properties of the two radial glia types. Dissecting eyes and brains separately instead of performing FAC sorting on dissociated whole heads would provide a level of spatial distinction between radial glia populations in future studies.

5.4. *Ice1* is indispensible for the Müller glia dedifferentiation response

In response to light damage, cells throughout the central retina were found to re-enter the cell cycle and stimulate a regenerative response that can restore the architecture and function of the zebrafish retina (Vihtelic and Hyde 2000). These cells were confirmed to be Müller glia, which dedifferentiate to a multipotent state and then divide to produce neural progenitor cells (Fausett and Goldman 2006). Blocking cell division during light lesioning via PCNA-morpholino knockdown triggers apoptosis in Müller glia and photoreceptors fail to regenerate (Matsuo et al. 2013). Similarly, interfering with Müller glia dedifferentiation suppresses subsequent proliferation. Knockdown of *ascl1a* and *lin-28* in zebrafish permits increased expression of *let-7*, which represses a number of regeneration-associated genes (Ramachandran, Fausett, et al. 2010).

Using a UV lesion paradigm, I demonstrated that *ice1* mutant Müller glia fail to undergo dedifferentiation response by 30hpl. Dedifferentiation of Müller glia typically occurs within 15 hours of injury, and proliferation begins within 2 days post injury (Ramachandran, Fausett, et al. 2010). Therefore, by 30hpl, Müller glia should be dedifferentiated and re-entering the cell cycle, as observed in the lesioned sibling retina. Due to low numbers of biological replicates, I was unable to determine statistical significance of mCherry+, EdU+, or mCherry+/EdU+ cell counts between UV40 siblings and mutants. However, there was consistently no EdU detection in the lesioned mutant retina, whereas EdU+ cells were consistently observed throughout the inner nuclear layer

of lesioned siblings including colabeled mCherry+ cells. It seems very likely that repetition of this experiment would confirm this disparity between siblings and mutants with statistical significance.

Connections have been previously drawn between splicing factor defects and photoreceptor cell death. For instance, the photoreceptor degeneration disease retinitis pigmentosa has often been linked to defects in pre-mRNA splicing caused by mutations in general splicing factors (Mordes et al. 2006; Yin et al. 2011). The loss of β-catenin observed at the apical boundary of the photoreceptor cell layer in *ice1* mutants suggests that there are polarity defects which could lead to functional defects over time. A closer examination of the photoreceptor cell phenotype in the *ice1* mutant may reveal a connection between

Overall, my data suggests that *ice1* is important for the dedifferentiation of Müller glia in response to photoreceptor cell death, drawing an important distinction between the effect of *ice1* deficiency in active versus quiescent neural stem cells.

5.5. Characterization of neural stem cells in the *ice1* mutant

The LEC component *ice1* is essential for neural stem cell maintenance in the zebrafish retina and brain. Using an *in vivo* loss-of-function mutant, I demonstrated that active neural stem cells in the CMZ of the retina and the PVZ of the forebrain exhibit cell cycle defects and increased levels of apoptosis, leading to progressive loss of stem cell compartments. RNA-seq analysis showed that *ice1* mutants have reduced transcript levels of cell cycle genes as well as visual and nervous system genes, which corroborates the observed mutant phenotype. Transcript abundance for splicing-associated genes was found to be increased, likely as a means of compensating for ice1 deficiency. Interestingly, RT-qPCR in isolated radial glial cells demonstrated that radial glia have a higher baseline level of snRNA genes, and that snRNA levels appear to be unaffected in

ice1 mutant radial glia. Instead, snRNA transcript levels appear to be reduced in differentiated neurons, suggesting that radial glia may be capable of maintaining snRNA levels despite ice1 deficiency. Furthermore, *ice1* appears to be necessary for activation of the early regenerative response in normally quiescent Müller glia in response to a UV lesion. My work demonstrates the importance of *ice1* for neural stem cell proliferation and survival. Investigating neural stem cell-specific effects serves to highlight key regulators in stem cell maintenance and function.

Chapter 6
References

Adler R, Canto-Soler MV. 2007. Molecular mechanisms of optic vesicle development: Complexities, ambiguities and controversies. Dev. Biol. 305:1–13.

Allende-Vega N, Dayal S, Agarwala U, Sparks A, Bourdon J-C, Saville MK. 2013. p53 is activated in response to disruption of the pre-mRNA splicing machinery. Oncogene 32:1–14.

Anwar D, Takahashi H, Watanabe M, Suzuki M, Fukuda S, Hatakeyama S. 2016. p53 represses the transcription of snRNA genes by preventing the formation of little elongation complex. Biochim. Biophys. Acta - Gene Regul. Mech. 1859:975–982.

Barbosa JS, Sanchez-gonzalez R, Di Giaimo R, Baumgart EV, Theis FJ, Götz M, Ninkovic J, Giaimo R Di, Baumgart EV, Theis FJ, et al. 2015. Live imaging of adult neural stem cell behavior in the intact and injured zebrafish brain. Science 348:789–93.

Bassett E a., Wallace V a. 2012. Cell fate determination in the vertebrate retina. Trends Neurosci. 35:565–573.

Bernardos RL, Barthel LK, Meyers JR, Raymond P. 2007. Late-Stage Neuronal Progenitors in the Retina Are Radial Muller Glia That Function as Retinal Stem Cells. J. Neurosci. 27:7028–7040.

Bezzi M, Teo SX, Muller J, Mok WC, Sahu SK, Vardy LA, Bonday ZQ, Guccione E. 2013. Regulation of constitutive and alternative splicing by PRMT5 reveals a role for Mdm4 pre-mRNA in sensing defects in the spliceosomal machinery. Genes Dev. 27:1903–1916.

Bibliowicz J, Gross JM. 2009. Expanded progenitor populations, vitreo-retinal abnormalities,

and Müller glial reactivity in the zebrafish leprechaun/patched2 retina. BMC Dev. Biol. 9:52.

Borday C, Cabochette P, Parain K, Mazurier N, Janssens S, Tran HT, Sekkali B, Bronchain O, Vleminckx K, Locker M, et al. 2012. Antagonistic cross-regulation between Wnt and Hedgehog signalling pathways controls post-embryonic retinal proliferation. Development 139:3499–3509.

Cayouette M, Poggi L, Harris WA. 2006. Lineage in the vertebrate retina. Trends Neurosci. 29:563–570.

Chapouton P, Webb KJ, Stigloher C, Alunni A, Adolf B, Hesl B, Topp S, Kremmer E, Bally-cuif L. 2011. Expression of Hairy / enhancer of split Genes in Neural Progenitors and Neurogenesis Domains of the Adult Zebrafish Brain. 1769:1748–1769.

Chen J, Wagner EJ. 2010. snRNA 3' end formation: the dawn of the Integrator complex. Biochem. Soc. Trans. 38:1082–7.

Cheng Y, Lund E, Kahan BW, Dahlberg JE. 1997. Control of mouse U1 snRNA gene expression during in vitro differentiation of mouse embryonic stem cells. Nucleic Acids Res. 25:2197–2204.

Dong Z, Yang N, Yeo SY, Chitnis A, Guo S. 2012. Intralineage Directional Notch Signaling Regulates Self-Renewal and Differentiation of Asymmetrically Dividing Radial Glia. Neuron 74:65–78.

Egloff S, O'Reilly D, Murphy S. 2008. Expression of human snRNA genes from beginning to end. Biochem. Soc. Trans. 36:590–4.

Fausett B V., Goldman D. 2006. A Role for 1 Tubulin-Expressing Muller Glia in Regeneration of the Injured Zebrafish Retina. J. Neurosci. 26:6303–6313.

Fischer AJ, Bosse JL, El-Hodiri HM. 2013. The ciliary marginal zone (CMZ) in development

and regeneration of the vertebrate eye. Exp. Eye Res. 116:199–204.

Folgueira M, Bayley P, Navratilova P, Becker TS, Wilson SW, Clarke JD. 2012. Morphogenesis underlying the development of the everted teleost telencephalon. Neural Dev. 7:32.

Hirsch CL, Akdemir ZC, Wang L, Jayakumaran G, Trcka D, Weiss A, Hernandez JJ, Pan Q, Han H, Xu X, et al. 2015. Myc and SAGA rewire an alternative splicing network during early somatic cell reprogramming. Genes Dev. 29:803–816.

Hu D, Smith E, Garruss A, Mohaghegh N, Varberg J, Lin C, Jackson J, Gao X, Saraf A, Florens L, et al. 2013. The little elongation complex functions at initiation and elongation phases of snRNA gene transcription. Mol. Cell 51:493–505.

Hutten S, Chachami G, Winter U, Melchior F, Lamond AI. 2014. A role for the Cajal-body-associated SUMO isopeptidase USPL1 in snRNA transcription mediated by RNA polymerase II. J. Cell Sci.

König H, Matter N, Bader R, Thiele W, Müller F. 2007. Splicing Segregation: The Minor Spliceosome Acts outside the Nucleus and Controls Cell Proliferation - Supplemental. Cell 131:718–729.

Kroehne V, Freudenreich D, Hans S, Kaslin J, Brand M. 2011. Regeneration of the adult zebrafish brain from neurogenic radial glia-type progenitors. Development 138:4831–4841.

Lenkowski JR, Raymond P a. 2014. Muller glia: Stem cells for generation and regeneration of retinal neurons in teleost fish. Prog. Retin. Eye Res. 40:94–123.

Li Q, Lee J-A, Black DL. 2007. Neuronal regulation of alternative pre-mRNA splicing. Nat. Rev. Neurosci. 8:819–831.

Lin C, Garrett AS, de Kumar B, Smith ER, Gogol M, Seidel C, Krumlauf R, Shilatifard A. 2011. Dynamic transcriptional events in embryonic stem cells mediated by the super elongation complex (SEC). Genes Dev. 25:1486–1498.

Lindsey BW, Darabie A, Tropepe V. 2012. The cellular composition of neurogenic periventricular zones in the adult zebrafish forebrain. J. Comp. Neurol. 520:2275–2316.

Listerman I, Bledau AS, Grishina I, Neugebauer KM. 2007. Extragenic accumulation of RNA polymerase II enhances transcription by RNA polymerase III. PLoS Genet. 3:2268–2277.

Livesey FJ, Cepko CL. 2001. Vertebrate neural cell-fate determination: Lessons from the retina. Nat. Rev. Neurosci. 2:109–118.

Lu Z, Matera AG. 2014. Developmental analysis of spliceosomal snRNA isoform expression. G3 (Bethesda). 5:103–10.

Luo Z, Lin C, Shilatifard A. 2012. The super elongation complex (SEC) family in transcriptional control. Nat. Rev. Mol. Cell Biol. 13:543–547.

MacDonald RB, Randlett O, Oswald J, Yoshimatsu T, Franze K, Harris W a. 2015. Muller glia provide essential tensile strength to the developing retina. J. Cell Biol. 210:1075–1083.

Machyna M, Heyn P, Neugebauer KM. 2013. Cajal bodies: Where form meets function. Wiley Interdiscip. Rev. RNA 4:17–34.

Marcus RC, L. DC, Easter SS. 1999. Neurogenesis in the visual system of embryonic and adult zebrafish (Danio rerio). Vis. Neurosci. 16:417–424.

Markmiller S, Cloonan N, Lardelli RM, Doggett K, Keightley M-C, Boglev Y, Trotter a. J, Ng a. Y, Wilkins SJ, Verkade H, et al. 2014. Minor class splicing shapes the zebrafish transcriptome

during development. Proc. Natl. Acad. Sci. 111:3062–3067.

Matera AG, Wang Z. 2014. A day in the life of the spliceosome. Nat. Rev. Mol. Cell Biol. 15:108–121.

Matsuo R, Yamagishi M, Wakiya K, Tanaka Y, Ito E. 2013. Inhibition of Muller Glial Cell Division Blocks Regeneration of the Light-Damaged Zebrafish Retina. Dev. Neurobiol. 73:609–620.

Ming G, Song H. 2005. Adult Neurogenesis in the Mammalian Central Nervous System. Annu. Rev. Neurosci. 28:223–250.

Mitrousis N, Tropepe V, Hermanson O. 2015. Post-translational modifications of histones in vertebrate neurogenesis. Front. Neurosci. 9:1–15.

Mordes D, Luo X, Kar A, Kuo D, Xu L, Fushimi K, Yu G, Sternberg P, Wu JY. 2006. Pre-mRNA splicing and retinitis pigmentosa. Mol. Vis. 12:1259–71.

Neuman de Vegvar HE, Lund E, Dahlberg JE. 1986. 3’ end formation of U1 snRNA precursors is coupled to transcription from snRNA promoters. Cell 47:259–266.

Patel A, Steitz J. 2003. Splicing double: insights from the second spliceosome. Nat. Rev. Mol. Cell Biol. 4:960–970.

Pessa HKJ, Will CL, Meng X, Schneider C, Watkins NJ, Perälä N, Nymark M, Turunen JJ, Lührmann R, Frilander MJ. 2008. Minor spliceosome components are predominantly localized in the nucleus. Proc. Natl. Acad. Sci. U. S. A. 105:8655–60.

Qin Z, Barthel LK, Raymond P a. 2009. Genetic evidence for shared mechanisms of epimorphic regeneration in zebrafish. Proc. Natl. Acad. Sci. U. S. A. 106:9310–9315.

Ramachandran R, Fausett B V., Goldman D. 2010. Ascl1a regulates Müller glia dedifferentiation and retinal regeneration through a Lin-28-dependent, let-7 microRNA signalling pathway. Nat. Cell Biol. 12:1101–1107.

Ramachandran R, Reifler A, Parent JM, Goldman D. 2010. Conditional gene expression and lineage tracing of tuba 1a expressing cells during zebrafish development and retina regeneration. J. Comp. Neurol. 518:4196–4212.

Raymond PA, Barthel LK, Bernardos RL, Perkowski JJ. 2006. Molecular characterization of retinal stem cells and their niches in adult zebrafish. BMC Dev. Biol. 6:36.

Rothenaigner I, Krecsmarik M, Hayes JA, Bahn B, Lepier A, Fortin G, Gotz M, Jagasia R, Bally-Cuif L. 2011. Clonal analysis by distinct viral vectors identifies bona fide neural stem cells in the adult zebrafish telencephalon and characterizes their division properties and fate. Development 138:1459–1469.

Shinobu N, Maeda T, Aso T, Ito T, Kondo T, Koike K, Hatakeyama M. 1999. Physical interaction and functional antagonism between the RNA polymerase II elongation factor ELL and p53. J. Biol. Chem. 274:17003–17010.

Smith ER, Lin C, Garrett AS, Thornton J, Mohaghegh N, Hu D, Jackson J, Saraf A, Swanson SK, Seidel C, et al. 2011. The Little Elongation Complex Regulates Small Nuclear RNA Transcription. Mol. Cell 44:954–965.

Sorfazlian N. 2015. Small nuclear RNA (snRNA) transcription elongation regulator , ice1 , is required for retinal progenitor cell maintenance.

Sprague J. 2006. The Zebrafish Information Network: the zebrafish model organism database.

Nucleic Acids Res. 34:D581–D585.

Stenkamp DL. 2011. The rod photoreceptor lineage of teleost fish. Prog. Retin. Eye Res. 30:395–404.

Stephens WZ, Senecal M, Nguyen M, Piotrowski T. 2010. Loss of adenomatous polyposis coli (apc) results in an expanded ciliary marginal zone in the zebrafish eye. Dev. Dyn. 239:2066–2077.

Strzelecka M, Trowitzsch S, Weber G, Lührmann R, Oates AC, Neugebauer KM. 2010. Coilin-dependent snRNP assembly is essential for zebrafish embryogenesis. Nat. Struct. Mol. Biol. 17:403–409.

Takahashi H, Takigawa I, Watanabe M, Anwar D, Shibata M, Tomomori-Sato C, Sato S, Ranjan A, Seidel CW, Tsukiyama T, et al. 2015. MED26 regulates the transcription of snRNA genes through the recruitment of little elongation complex. Nat. Commun. 6:5941.

Trede NS, Medenbach J, Damianov A, Hung L-H, Weber GJ, Paw BH, Zhou Y, Hersey C, Zapata A, Keefe M, et al. 2007. Network of coregulated spliceosome components revealed by zebrafish mutant in recycling factor p110. Proc. Natl. Acad. Sci. U. S. A. 104:6608–6613.

Valadkhan S. 2010. Role of the snRNAs in spliceosomal active site. RNA Biol. 7:345–353.

Vazquez-Arango P, Vowles J, Browne C, Hartfield E, Fernandes HJR, Mandefro B, Sareen D, James W, Wade-Martins R, Cowley SA, et al. 2016. Variant U1 snRNAs are implicated in human pluripotent stem cell maintenance and neuromuscular disease. Nucleic Acids Res. 44:10960–10973.

Vihtelic TS, Hyde DR. 2000. Light induced rod and cone cell death and regeneration in the adult

albino zebrafish (Danio rerio) retina. J. Neurobiol. 44:289–307.

Wan Y, Almeida AD, Rulands S, Chalour N, Muresan L, Wu Y, Simons BD, He J, Harris W. 2016. The ciliary marginal zone of the zebrafish retina: clonal and time-lapse analysis of a continuously growing tissue. Development:1099–1107.

Wehman AM, Staub W, Meyers JR, Raymond PA, Baier H. 2005. Genetic dissection of the zebrafish retinal stem-cell compartment. Dev. Biol. 281:53–65.

Yap K, Lim ZQ, Khandelia P, Friedman B, Makeyev E V. 2012. Coordinated regulation of neuronal mRNA steady-state levels through developmentally controlled intron retention. Genes Dev. 26:1209–1223.

Yin J, Brocher J, Fischer U, Winkler C. 2011. Mutant Prpf31 causes pre-mRNA splicing defects and rod photoreceptor cell degeneration in a zebrafish model for Retinitis pigmentosa. Mol. Neurodegener. 6:56.

Chapter 7
Appendices

Appendix A. *GO term enrichment of differentially expressed genes detected by RNA-sequencing in 4dpf whole heads of* ice1 *mutants compared with siblings.*
Up-regulation/down-regulation of genes with log2 fold change in mutants compared with siblings ($p < 0.05$).

Function Category	*GO Term*	Up-regulated	Down-regulated
anatomical structure development	anatomical structure development	--	+
	chordate embryonic development	--	+
	multicellular organismal development	--	+
	tissue development	--	+
apoptosis	extrinsic apoptotic signaling pathway via death domain receptors	+	--
	intrinsic apoptotic signaling pathway in response to DNA damage by p53 class mediator	+	--
	positive regulation of apoptotic process	+	--
	regulation of cysteine-type endopeptidase activity involved in apoptotic process	+	--
cell communication	cell communication	--	+
cell cycle	centriolar satellite	+	--
	meiotic nuclear division	+	--
	cell cycle	--	+
	cell division	--	+
	cleavage furrow formation	--	+
	HAUS complex	--	+
	mitotic cell cycle	--	+
	mitotic chromosome condensation	--	+
	mitotic cytokinesis	--	+
	mitotic nuclear division	--	+
	mitotic sister chromatid segregation	--	+
	mitotic spindle assembly checkpoint	--	+
	mitotic spindle midzone assembly	--	+
	mitotic spindle organization	--	+
	Ndc80 complex	--	+
	regulation of cell cycle	--	+
	regulation of G2/M transition of mitotic cell cycle	--	+
	regulation of mitotic cell cycle, embryonic	--	+

	spindle assembly	--	+
	spindle microtubule	--	+
cell differentiation	cell dedifferentiation	--	+
	cell differentiation	--	+
	transdifferentiation	--	+
cell growth	positive regulation of cell growth	+	--
cell junction	cell-substrate junction assembly	+	--
cell polarity	establishment of cell polarity	+	--
chromatin/chromosome	CAF-1 complex	--	+
	centromere complex assembly	--	+
	centrosome organization	--	+
	chromatin	--	+
	chromatin assembly	--	+
	chromatin binding	--	+
	chromatin modification	--	+
	chromatin organization	--	+
	chromosome	--	+
	chromosome condensation	--	+
	chromosome passenger complex	--	+
	chromosome segregation	--	+
	chromosome separation	--	+
	chromosome, centromeric region	--	+
	condensed chromosome	--	+
	condensed chromosome kinetochore	--	+
	condensin complex	--	+
	histone binding	--	+
	histone H3-K9 methylation	--	+
	kinetochore	--	+
	nucleosome	--	+
	nucleosome assembly	--	+
	NuRD complex	--	+
	protein-chromophore linkage	--	+
cytoskeletal	inner dynein arm assembly	+	--
	outer dynein arm assembly	+	--
	regulation of actin filament polymerization	+	--
	intermediate filament	--	+
	kinesin complex	--	+
	microtubule	--	+
	microtubule binding	--	+
	microtubule cytoskeleton organization	--	+
	microtubule motor activity	--	+
DNA binding	chromatin DNA binding	--	+

	core promoter binding	--	+
	DNA binding	--	+
	DNA binding, bending	--	+
	DNA clamp loader activity	--	+
	RNA polymerase II regulatory region sequence-specific DNA binding	--	+
	sequence-specific DNA binding	--	+
DNA metabolic process	3'-5' DNA helicase activity	--	+
	alpha DNA polymerase:primase complex	--	+
	base-excision repair	--	+
	DNA methylation	--	+
	DNA methylation on cytosine	--	+
	DNA recombination	--	+
	DNA repair	--	+
	DNA replication	--	+
	DNA replication factor C complex	--	+
	DNA replication initiation	--	+
	DNA replication, removal of RNA primer	--	+
	DNA-dependent DNA replication	--	+
	DNA-directed DNA polymerase activity	--	+
	double-strand break repair via break-induced replication	--	+
	GINS complex	--	+
	leading strand elongation	--	+
	MCM complex	--	+
	mismatch repair	--	+
	regulation of DNA replication	--	+
	replication fork protection complex	--	+
	translesion synthesis	--	+
enzyme activity	catalytic activity	--	+
	exogenous drug catabolic process	--	+
	nucleoside kinase activity	--	+
	ATP-dependent helicase activity	--	+
	DNA-dependent ATPase activity	--	+
	single-stranded DNA-dependent ATPase activity	--	+
	hydrolase activity	--	+
	hydrolase activity, acting on acid anhydrides, in phosphorus-containing anhydrides	--	+
	hydrolase activity, acting on carbon-nitrogen (but not peptide) bonds, in cyclic amides	--	+
	carbamoyl-phosphate synthase (ammonia) activity	--	+

	carbamoyl-phosphate synthase (glutamine-hydrolyzing) activity	--	+
	2-methylcitrate dehydratase activity	+	--
	aconitate decarboxylase activity	+	--
	DNA-(apurinic or apyrimidinic site) lyase activity	--	+
	lyase activity	--	+
	3'-5'-exodeoxyribonuclease activity	--	+
	endonuclease activity	--	+
	nuclease activity	--	+
	carboxyl- or carbamoyltransferase activity	--	+
	estrone sulfotransferase activity	--	+
	telomerase activity	--	+
	transaminase activity	--	+
	transferase activity	--	+
enzyme regulator activity	cyclin-dependent protein serine/threonine kinase regulator activity	--	+
	serine-type endopeptidase inhibitor activity	--	+
homeostasis	cellular water homeostasis	--	+
immune system	activation of innate immune response	+	--
	inflammatory response	+	--
	innate immune response	+	--
	interferon-gamma receptor binding	+	--
	MyD88-dependent toll-like receptor signaling pathway	+	--
	positive regulation of inflammatory response	+	--
	positive regulation of lymphangiogenesis	+	--
	regulation of cytokine secretion	+	--
	regulation of inflammatory response	+	--
	toll-like receptor 2 signaling pathway	+	--
	B cell differentiation	--	+
	mast cell activation	--	+
	T cell differentiation in thymus	--	+
	V(D)J recombination	--	+
methylation	methylation	--	+
	methyltransferase activity	--	+
	S-adenosylmethionine-dependent methyltransferase activity	--	+
molecular binding	phosphatidylinositol-3,4-bisphosphate binding	+	--
	protease binding	+	--
	Pyrin domain binding	+	--
	heme binding	--	+
	iron ion binding	--	+

	oxygen binding	--	+
	poly(A) RNA binding	--	+
	polysaccharide binding	--	+
	purine nucleotide binding	--	+
	pyridoxal phosphate binding	--	+
nervous system	cell differentiation in spinal cord	--	+
	diencephalon development	--	+
	forebrain neuron differentiation	--	+
	generation of neurons	--	+
	hindbrain development	--	+
	midbrain development	--	+
	nervous system development	--	+
	neural crest cell development	--	+
	neural crest formation	--	+
	neurogenesis	--	+
	neuron cellular homeostasis	--	+
	Notch signaling pathway	--	+
	positive regulation of neurogenesis	--	+
	ventral spinal cord interneuron differentiation	--	+
	visual perception	--	+
response to stress	angiogenesis involved in wound healing	+	--
	defense response	+	--
	DNA damage response, signal transduction by p53 class mediator resulting in transcription of p21 class mediator	+	--
	positive regulation of insulin secretion involved in cellular response to glucose stimulus	+	--
	response to gamma radiation	+	--
	response to mechanical stimulus	+	--
	response to molecule of bacterial origin	+	--
	response to starvation	+	--
	response to virus	+	--
	response to wounding	+	--
	response to X-ray	+	--
	cellular response to antibiotic	--	+
	cellular response to DNA damage stimulus	--	+
	response to yeast	--	+
ribosome	5S rRNA binding	--	+
	cytosolic large ribosomal subunit	--	+
	cytosolic small ribosomal subunit	--	+

	endonucleolytic cleavage to generate mature 3'-end of SSU-rRNA from (SSU-rRNA, 5.8S rRNA, LSU-rRNA)	--	+
	ribonucleoprotein complex	--	+
	ribosomal large subunit assembly	--	+
	ribosomal small subunit assembly	--	+
	ribosomal small subunit biogenesis	--	+
	ribosome	--	+
	small ribosomal subunit	--	+
	structural constituent of ribosome	--	+
RNA	RNA metabolic process	--	+
signal transduction	cellular response to organic cyclic compound	+	--
	cytokine activity	+	--
	glucagon receptor binding	+	--
	I-kappaB kinase/NF-kappaB signaling	+	--
	JAK-STAT cascade	+	--
	negative regulation of I-kappaB kinase/NF-kappaB signaling	+	--
	positive regulation of JAK-STAT cascade	+	--
	protein kinase A signaling	+	--
	regulation of retinoic acid receptor signaling pathway	+	--
	response to cytokine	+	--
	response to lipopolysaccharide	+	--
	thrombin receptor activity	+	--
	thrombin receptor signaling pathway	+	--
	cellular response to estrogen stimulus	--	+
splicing	Cajal body	+	--
	cytoplasmic mRNA processing body	+	--
	gene silencing by RNA	+	--
	mRNA splicing, via spliceosome	+	--
	RNA splicing	+	--
	spliceosomal complex	+	--
	spliceosomal tri-snRNP complex assembly	+	--
	U1 snRNP	+	--
	U2 snRNA binding	+	--
	U2 snRNP	+	--
	U4 snRNP	+	--
	U4/U6 x U5 tri-snRNP complex	+	--
	U5 snRNP	+	--
	U6 snRNA binding	+	--
transcription	DNA-directed RNA polymerase II, core complex	+	--

	negative regulation of transcription from RNA polymerase II promoter	--	+
	positive regulation of sequence-specific DNA binding transcription factor activity	--	+
	regulation of transcription, DNA-templated	--	+
	RNA polymerase II transcription regulatory region sequence-specific DNA binding transcription factor activity involved in negative regulation of transcription	--	+
	sequence-specific DNA binding transcription factor activity	--	+
	transcription factor complex	--	+
	transcription, DNA-templated	--	+
translation	positive regulation of translational initiation	+	--
	cytoplasmic translation	--	+
	translation	--	+
visual system	eye development	--	+
	lens development in camera-type eye	--	+
	photoreceptor activity	--	+
	photoreceptor outer segment	--	+
	phototransduction	--	+
	retina layer formation	--	+
	retina morphogenesis in camera-type eye	--	+
	structural constituent of eye lens	--	+

Appendix B. *GO term enrichment of differential intron retention detected by RNA-sequencing in 4dpf whole heads of* ice1 *mutants compared with siblings.*
Intron retention coefficient was determined as intron RPKM/coding sequence RPKM.
Significant differences in mutants were determined by t-test ($p < 0.05$).

Function Category	GO Term	Up-regulated	Down-regulated
cell cycle	negative regulation of cytokinesis	+	--
	regulation of cell division	--	+
cell junction	cell-substrate junction assembly	--	+
cell polarity	regulation of establishment of cell polarity	--	+
chromatin/chromosome	transcriptionally active chromatin	+	--
dephosphorylation	dephosphorylation	--	+
development	positive regulation of gastrulation	--	+
nervous system	axon extension	+	--
response to stress	cellular response to ionizing radiation	+	--
	positive regulation of wound healing	+	--
	Mre11 complex	+	--
	intrinsic apoptotic signaling pathway in response to endoplasmic reticulum stress	+	--
	cellular response to light stimulus	--	+
	response to metal ion	--	+
	response to zinc ion	--	+
RNA metabolism	Ski complex	+	--
signal transduction	cellular response to epidermal growth factor stimulus	+	--
	negative regulation of canonical Wnt signaling pathway involved in cardiac muscle cell fate commitment	--	+
	G-protein coupled glutamate receptor signaling pathway	--	+
transcription	Cdc73/Paf1 complex	+	--
transport	chloride channel regulator activity	+	--
	positive regulation of sodium ion transport	+	--
	positive regulation of transporter activity	+	--
	post-Golgi vesicle-mediated transport	+	--
	insulin-responsive compartment	--	+
	transport vesicle membrane	--	+
visual system	eye photoreceptor cell differentiation	--	+

Appendix C. *GO term enrichment of differentiall 3' UTR retention detected by RNA-sequencing in 4dpf whole heads of* ice1 *mutants compared with siblings.*
3'UTR retention coefficient was determined as 3' UTR RPKM/coding sequence RPKM.
Significant differences in mutants were determined by t-test ($p < 0.05$).

Function Category	GO Term	Up-regulated	Down-regulated
cell cycle	mitotic sister chromatid segregation	--	+
cell division	cell division	--	+
chromatin/chromosome	nuclear euchromatin	--	+
cytoskeletal	microtubule binding	--	+
	actin filament depolymerization	+	--
nervous system	dendritic shaft	--	+
	growth cone	--	+
	Notch receptor processing	--	+
	regulation of synaptic transmission, glutamatergic	+	--
response to stress	multicellular organismal response to stress	+	--
RNA metabolism	mRNA pseudouridine synthesis	+	--
signal transduction	regulation of insulin receptor signaling pathway	--	+
	group II metabotropic glutamate receptor activity	+	--
	G-protein coupled glutamate receptor signaling pathway	+	--
splicing	negative regulation of mRNA splicing, via spliceosome	--	+
	positive regulation of mRNA splicing, via spliceosome	--	+
	supraspliceosomal complex	--	+
transcription	core promoter binding	--	+
	positive regulation of transcription via serum response element binding	+	--
visual system	absorption of visible light	--	+
	compound eye photoreceptor development	--	+
	ciliary rootlet	--	+
	photoreceptor connecting cilium	--	+
	detection of visible light	--	+
vitamin	11-cis retinal binding	--	+
	all-trans retinal binding	--	+